Petroleum Science 19 (2022) 74–90

Contents lists available at ScienceDirect

Petroleum Science

journal homepage: www.keaipublishing.com/en/journals/petroleum-science

Original Paper

Source of silica and its implications for organic matter enrichment in the Upper Ordovician-Lower Silurian black shale in western Hubei Province, China: Insights from geochemical and petrological analysis

Quan-Sheng Cai [a, b, c], Ming-Yi Hu [a, *], Bao-Min Zhang [c], Ngong Ngia [a, d], An Liu [c], Rui-Quan Liao [e], Oumar Kane [a], Hai Li [c], Zhong-Gui Hu [a], Qing-Jie Deng [a], Jun-Jun Shen [a]

[a] School of Geosciences, Yangtze University, Wuhan, Hubei 430100, China
[b] Key Laboratory of Tectonics and Petroleum Resources of Ministry of Education (China University of Geosciences), Wuhan, Hubei 430074, China
[c] Wuhan Center of China Geological Survey, Wuhan, Hubei 430205, China
[d] Department of Geology, University of Buea, P.O. Box 63, Buea, Southwest, Cameroon
[e] School of Petroleum Engineering, Yangtze University, Wuhan, Hubei 430100, China

ARTICLE INFO

Article history:
Received 26 September 2020
Accepted 27 June 2021
Available online 23 October 2021

Edited by Jie Hao and Teng Zhu

Keywords:
Biogenic silica
Terrigenous siliciclastic input
Organic matter enrichment
Black shale
Continental shelf
Sea-level change
Wufeng-Longmaxi formations

ABSTRACT

To improve the understanding of the relationship between silica source and organic matter accumulation, the origin of silica and its implications for organic matter enrichment in the Upper Ordovician-Lower Silurian (O_3w-S_1l) black shale in western Hubei Province in the middle Yangtze area, were investigated through geochemical and petrological analyses. The results show that the O_3w-S_1l black shale is mainly composed of five lithofacies with varying graptolite abundance, total organic carbon (TOC), and silica contents. Biogenic silica and terrigenous siliciclastic input constitute the main silica sources in O_3w-S_1l black shale and they exhibit an upward inverse variation trend interpreted to be related to sea-level changes. Moreover, with the increase in biogenic silica content or decrease in terrigenous siliciclastic input, TOC values in black shale initially rise and then fall, which is different from originally expected simple linear relationship. We infer that organic matter enrichment and the distribution of silica from different origins are controlled by sea-level changes and variations in terrigenous input in a continental shelf with little hydrothermal influence. An environment with appropriate sea level and terrigenous input should be most favorable for organic matter accumulation, rather than one with excessive high sea level and less terrigenous input.

1. Introduction

Siliceous minerals are the primary components of marine organic-rich shale and play an important role in evaluating shale reservoir quality (Dean et al., 1985; Murray et al., 1994; Schieber et al., 2000; Kennedy et al., 2002; Li et al. 2013, 2018; Keil and Mayer, 2014; Wang et al., 2014; Han et al. 2016, 2018; Milliken et al., 2017; Zhao et al. 2017a, 2017b; Dong et al., 2019; Xi et al., 2019; Ma et al., 2020; Pan et al., 2020). However, there are multiple sources for silica in marine deposits, including terrigenous, hydrothermal, and biogenic silica (Bio-Si) (Boström, 1973; Adachi et al., 1986; Murray et al., 1994; Harris et al., 2011; Milliken et al., 2016; Yang et al., 2018; Zhang et al., 2018; Jiang et al., 2019; Khan et al., 2019; Li et al., 2019; Liu et al., 2019; Cai et al., 2020). Different silica sources have various implications for marine environments and shale reservoir characteristics. Siliceous materials with biogenic origins are more enriched along continental margins (Khan et al., 2019; Liu et al., 2019), hydrothermal silica is common in ocean basins and ocean rift environments (Olivarez et al., 1989; Murray et al., 1994; Chen et al., 2006; Zhou et al., 2006; Qiu et al., 2011; Zhang et al., 2018), and proximal sediments contain large amounts of terrigenous silica (Qiu et al., 2018; Yang et al., 2018; Wu et al., 2020). Most siliceous minerals can improve the shale brittleness index, but Bio-Si enrichment is more favorable to forming natural and artificial fractures than other forms of silica (Zeng et al., 2013; Zhao et al., 2017a; Han et al., 2018; Xi et al., 2019). Moreover,

* Corresponding author.
E-mail address: humingyi65@163.com (M.-Y. Hu).

https://doi.org/10.1016/j.petsci.2021.10.012

in previous researches, Bio-Si content of marine black shale has demonstrated a good linear correlation with total organic carbon (TOC), and can be used to infer paleoproductivity (Nelson et al., 1995; Zhang et al., 2018; Khan et al., 2019; Li et al., 2019; Wang et al., 2019). Unlike Bio-Si, terrigenous silica is usually considered to play a negative role in organic matter accumulation due to dilution and the negative relationship with TOC (Murphy et al., 2000; Sageman et al., 2003; Ji et al., 2020). However, our new research shows that organic matter in marine shale with the highest Bio-Si content or least terrigenous siliciclastic input is not the most enriched, indicating that there may be a more complex relationship between different-origin silica and organic matter accumulation, rather than a simple linear correlation.

To improve the understanding of the relationship between silica sources and organic matter enrichment, three sections (including two drilling cores and one field outcrop section) mainly composed of the Upper Ordovician Wufeng Formation (O_3w) and Lower Silurian Longmaxi Formation (S_1l) black shale located in western Hubei Province, South China were examined. The main goals of this study are: (1) to systematically analyze the different origins of silica in the O_3w-S_1l black shale and their relationships to organic matter enrichment utilizing petrological and geochemical data and (2) to discuss the distribution pattern of different-origin silica and organic matter in a continental shelf environment to improve the understanding of organic matter enrichment mechanisms.

2. Geological background

The study area is located in the western Hubei Province and belongs to the western portion of the Middle Yangtze Platform adjacent to the Sichuan Basin (Fig. 1a). As a part of the eastern slope of the ancient Huangling Uplift, the Pre-Cambrian Nanhua-Early Paleozoic Silurian strata in the study area are exposed and the Global Stratotype Section and Point (GSSP) for the base Hirnantian has been established (Fig. 1b). In recent years, the O_3w-S_1l black shale in the study area has become a hotspot for shale gas exploration in South China due to its immature faults and relatively stable tectonic environment (Li et al., 2012; Chen et al., 2018; Zhang et al., 2019).

From the Late Ordovician to the Early Silurian, the Yangtze Platform underwent non-uniform subsidence and evolved into a semi-enclosed continental shelf surrounded by the Qianzhong, Xuefeng and Chuanzhong uplifts, with gradually intensifying compression and collision between the Cathaysia and Yangtze blocks during the Kwangsian Orogeny (Fig. 1a) (Chen et al., 2004; Su et al. 2007, 2009; Yang et al., 2020). From the beginning of the late Katian to the early Aeronian, the Yangtze Sea experienced several significant sea-level variations related to tectonic subsidence and continental glaciation (Yan et al., 2010; Gorjan et al., 2012; Liu et al. 2016, 2017), which resulted in the widespread organic-rich black shale deposits of the O_3w and lower part of the S_1l (Chen et al., 2004; Su et al., 2007; Fan et al., 2011; Xiao et al., 2015). The O_3w-S_1l black rock series in the study area is approximately 20 m thick and is primarily composed of carbonaceous shale with ubiquitous siliceous minerals, graptolites, and radiolarians, while the middle and upper S_1l are dominated by greyish-green mudstone and siltstone formed in a shallow marine shelf environment caused by sea-level fall resulting from continuous tectonic uplift (Chen et al., 2004; Huang et al., 2018).

3. Samples and methods

One hundred and two (102) samples were collected from the O_3w-S_1l black rock series in three sections, including 20 samples from the lower S_1l in the Hengshi section, 28 samples from Well Yy2, and 54 samples from Well Yy3 (Fig. 2). Among them, 60 samples were analyzed for element concentration, and a subset of 57 samples was analyzed for TOC. Mineral composition was analyzed in 63 samples, and the graptolite abundance in 54 samples from Well Yy3 was also counted. Samples were sent to the Zhongnan Mineral Resources Supervision and Test Center, Wuhan Center of China Geological Survey (WHCGS) for geochemical analysis, and the mineral analysis was completed at Irock Technology Co., Ltd.

At the WHCGS, all samples were powdered to 200 mesh for geochemical analysis. Samples were analyzed for TOC using a CS844-3250 carbon and sulfur analyzer with an analytical

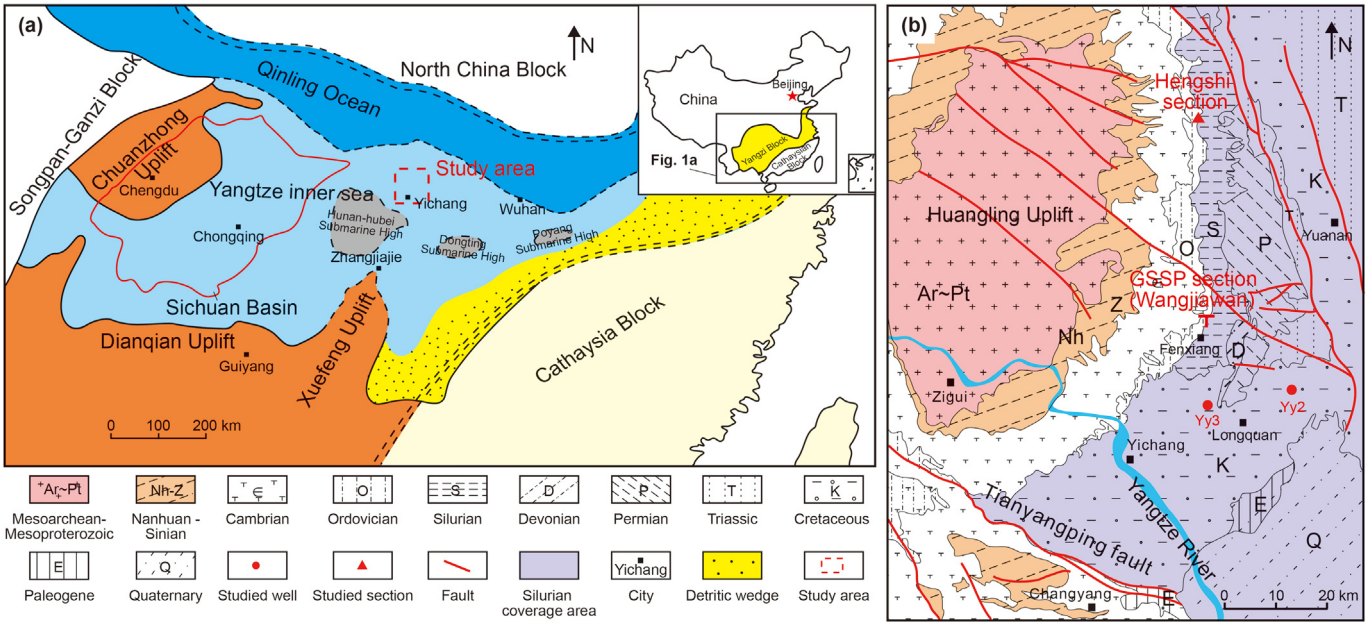

Fig. 1. (a) Paleogeographic map of the Yangzte Block during the Late Ordovician-Early Silurian transition (Modified from Chen et al., 2004 and Zhang et al., 2018). (b) Geological map of the study area showing sampling locations.

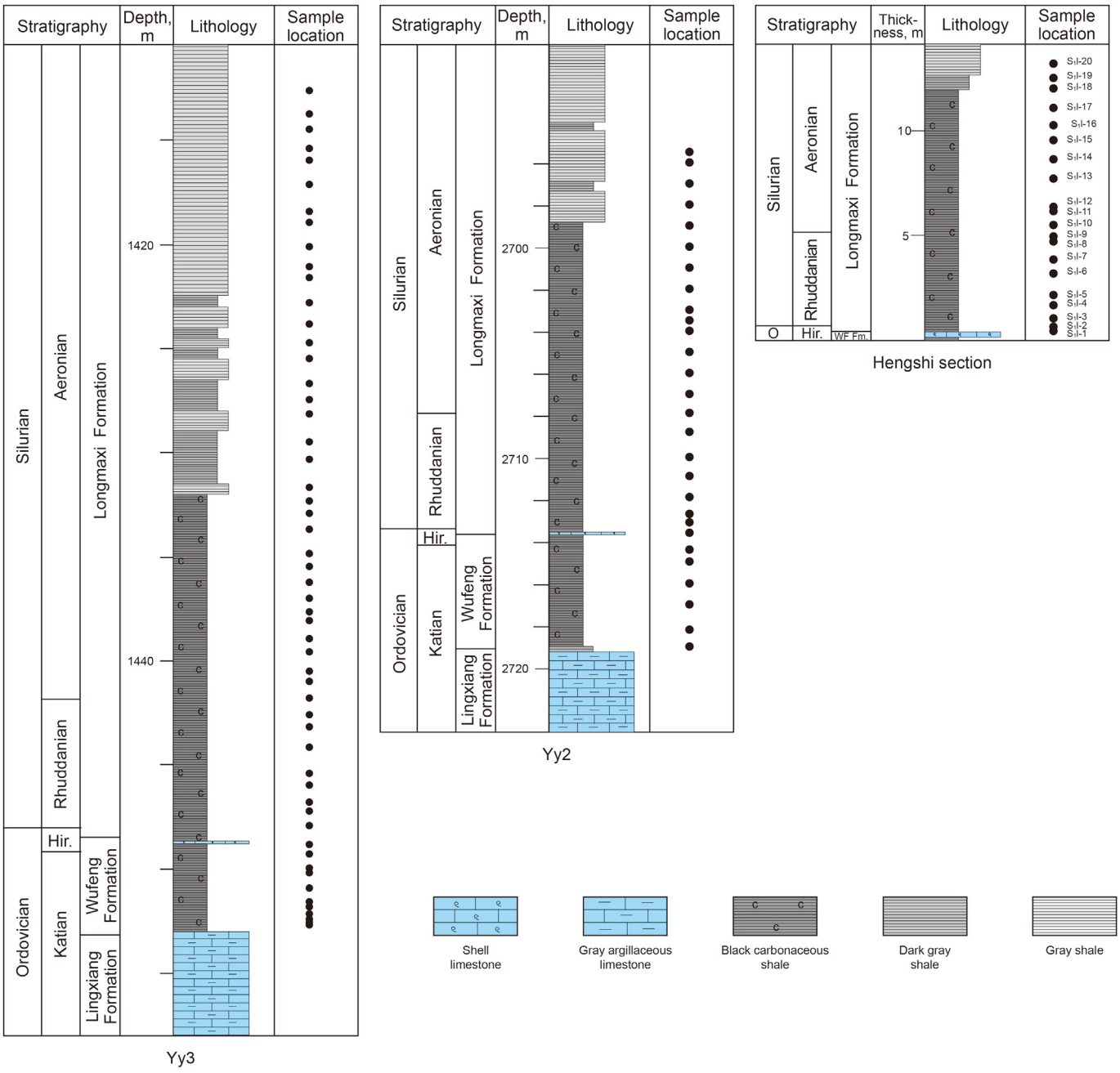

Fig. 2. Stratigraphic columns of the O_3w-S_1l series in wells Yy3 and Yy2, and in the Hengshi section showing the sample location. Hir = Hirnantian, O = Ordovician, and WF Fm = Wufeng Formation.

uncertainty of <0.5%. For major element analysis, the major oxides were measured using a Philips PW2404 spectrometer following the Chinese national standard GB/T 14506. Trace and rare elements were analyzed using an Element XR ICP-MS with an analytical uncertainty of <0.5%, following operational procedures detailed by Li et al. (2015).

In IROCK Technology Co., Ltd, mineral compositions were measured using a Bruker D8 advanced automated powder diffractometer. Powdered samples were scanned from 5° to 90° at 2°/min with a step size of 0.02°. Minerals were identified from the diffractograms and their contents were obtained by using EVA Software. Additionally, a high-resolution field emission scanning electron microscope (FE-SEM) equipped with an energy dispersive spectrometer (EDS) was also used to identify minerals.

The O_3w-S_1l black shale cores of Well Yy3 are 7.5 cm in diameter. Hence, it is possible to estimate the graptolite abundance using the number of graptolites on a bedding surface (NGC) and the ratio between total graptolite surface area and core bedding surface area (RGC). Here, the variations in core bedding surface area can be overlooked because of the low stratigraphic dip.

For analyzing silica sources, excess silica (Si_{excess}) content is adopted to represent the total silica content excluding normal terrigenous silica deposits (Murray and Leinen, 1996; Zhang et al., 2018), which can be calculated as follows:

$$Si_{excess} = Si_s - \left[(Si/Al)_{paas} \times Al_s\right]$$

where Si_s and Al_s refer to the silicon and aluminum contents in samples, respectively. $(Si/Al)_{paas}$ is the average ratio of Si/Al in the Post-Archean Australian Shale (PAAS), which is 3.11 (Taylor and Mcclennans, 1985).

The chemical index of alteration (CIA) is often used to evaluate terrigenous detrital input and weathering conditions (Nesbitt and Young, 1982; Price and Velbel, 2003; Liu et al., 2017), which can be calculated by the following formula:

$$CIA = 100 \times [Al_2O_3/(Al_2O_3 + CaO^* + Na_2O + K_2O)]$$

Here, CaO* only represents the CaO in silicate minerals, which can be amended by $CaO^* = \min[X(CaO) - X(P_2O_5) \times 10/3, X(Na_2O)]$ (Nesbitt and Young, 1982; Mclennan, 1993), where X refers to the corresponding oxide content.

4. Results

4.1. Mineral composition

Petrographic observations showed that the O_3w and lower S_1l in the study area were primarily dominated by organic-rich black shale with locally interbedded dark-gray shale, thin-bedded siltstone, and argillaceous limestone. Analytical data from 63 samples from the Yy2 and Yy3 wells, as well as the Hengshi section revealed that the black shale consists primarily of quartz and clay minerals with secondary carbonate minerals, feldspar, and pyrite (Table 1).

In the black shale samples, quartz content ranged from 27.5% to 91.2% (with an average of 46.7%), and the average quartz content of samples in the O_3w and the lower S_1l was 51.8% and 45.8%, respectively. In thin sections, ubiquitous angular quartz was found (Fig. 3a and b), as well as biological-related quartz (Fig. 3c, d, e). Clay minerals were mainly composed of illite and a mixture of illite/smectite ranging from 5.3% to 65.13% with an average of 39.14% (Fig. 3f), showing a gradually increasing upward trend. Feldspar dominated by plagioclase and K-feldspar presented values ranging from 0% to 22.1%, with an average of 7.65% (Fig. 3f and g). Carbonate minerals dominated by ferrodolomite and some calcite were primarily distributed in the lower part of the O_3w-S_1l black shale (Fig. 3h). Dispersed pyrite was widely distributed in all samples, and pyrite framboids were common in SEM images (Fig. 3i).

The collected samples were classified into five lithofacies based on mineral composition: siliceous shale, mixed siliceous shale, mixed shale, mixed argillaceous shale, and argillaceous shale (Fig. 4). The lithofacies showed significant upward variations throughout the studied profiles. Siliceous shale and mixed siliceous shale were primarily present in the Katian to Rhuddanian sections, while mixed shale was primarily developed in the Hirnantian section. Mixed argillaceous shale and argillaceous shale were widely distributed in the Aeronian section (Fig. 4). In addition, the shale color in each profile gradually changed from black to gray vertically.

4.2. Biological fossils

The O_3w-S_1l black shale in the study area contains abundant fossils, including graptolites and radiolarians, as well as some spongy spicules and shells (Fig. 5). Graptolites, dominated by planktonic graptolites, are primarily distributed in the mixed siliceous shale (Fig. 5c), while are less common in siliceous and argillaceous shales (Fig. 5a, e). Statistical data from 54 samples from well Yy3 showed that NGC ranged from 0 to 90, and RGC ranged from 0 to 70%. Graptolite abundance in the O_3w-S_1l black shale gradually decreases upward (Fig. 4), and shell fossils are common in the middle O_3w to lower S_1l (Fig. 5f). The argillaceous limestone with abundant Hirnantia fauna (known as the Guanyinqiao bed) in the black shale is commonly used as a lithological marker to distinguish O_3w and S_1l (Rong et al., 2002; Chen et al., 2004; Zhan et al., 2010; Fan et al., 2011). Siliceous radiolarians are visible in the black shale with high silica content (Fig. 5g), whereas radiolarians are rare in the clay-rich argillaceous shale (Fig. 5h and i).

4.3. Total organic carbon

According to the analyzed data from the 57 collected samples, the TOC values varied from 0.36% to 6.38% with an average of 2.47%, and most TOC values ranged from 1% to 4% (Fig. 6a). In the three studied sections, the black shale TOC decreased gradually from bottom to top. In addition, different lithofacies showed significant variations in TOC values (Fig. 6b). The TOC of mixed argillaceous shale ranged from 0.36% to 3.32% (averaging 1.09%), TOC of mixed siliceous shale ranged from 0.98% to 5.53% with an average of 2.74%, and siliceous shale had a relatively higher TOC content ranging from 1.28% to 6.38% with an average of 3.16%. In general, the TOC value showed an apparent increase from clay-rich shale to silica-rich shale; however, some shale samples with the highest silica content had low TOC values (Fig. 6b).

4.4. Major elements

Major element analysis indicated that SiO_2 and Al_2O_3 are the primary constituents in the O_3w-S_1l black shale. SiO_2 ranged from 28.27% to 88.69% and averaged 65.91% (Table 2), showing a gradual upward decrease. Shale samples with high SiO_2 content were primarily distributed in the Katian and Rhuddanian sections. As an effective proxy for estimating terrigenous input, Al_2O_3 concentrations varied from 2.16% to 18.4% with an average of 12.6%, showing an increasing upward trend (Table 2). Fe_2O_3, FeO, MgO, and K_2O were the second most abundant oxides with average contents of 2.51%, 2.46%, 1.97%, and 3.16%, respectively. CaO contents in most samples were <1%, as were Na_2O and P_2O_5.

According to the formula for excess silica (Si_{excess}) content, the calculated Si_{excess} in samples ranged from 0% to 33.35% with an average of 9.89% and showed an abrupt upward decrease in the three study profiles. The CIA values, which are commonly used to analyze paleoclimate changes and weathering intensity, showed an increase upward and ranged from 66.57 to 77.53 with an average of 73.43 (Table 2).

4.5. Trace and rare elements

Geochemical proxies, including sensitive trace element concentrations and their ratios, are widely used for paleo-marine condition reconstruction (Jones and Manning, 1994; Algeo and Maynard, 2004; Tribovillard et al., 2006). In this research, we chose U/Th and V/Cr to identify paleo-marine redox environment, and the geochemical proxies Ni/Al and P/Al ratios were used as paleoproductivity indicators (Table 2).

U/Th and V/Cr are redox-sensitive indicators (Lewan and Maynard, 1982; Jones and Manning, 1994; Ross and Bustin, 2009). For anoxic conditions, the U/Th and V/Cr ratios are usually >1.25 and 4.25. For dysoxic environments, the U/Th ratios range from 0.75 to 1.25 and V/Cr ratios generally range from 2.0 to 4.25. U/Th ratios <0.75 and V/Cr ratios <2.0 indicate oxic conditions (Wignall and Myers, 1988; Jones and Manning, 1994). U/Th and V/Cr ratios of the samples from O_3w-S_1l black shale had similar variation trends,

Table 1
Mineral composition of the O_3w-S_1l black shale from the Yy2 and Yy3 wells, as well as the Hengshi Section.

Section name	Sample location	Clay mineral, %	Quartz, %	Albite, %	K-feldspar, %	Pyrite, %	Carbonate minerals, %
Yy3	1415.40 m	64.90	27.80	6.00	0	0	1.36
Yy3	1418.91 m	59.50	30.50	8.60	0	1.50	0
Yy3	1422.80 m	63.20	29.30	6.30	0	1.30	0
Yy3	1432.31 m	61.20	31.30	5.70	0	1.90	0
Yy3	1432.95 m	61.60	31.40	7.00	0	0	0
Yy3	1434.84 m	55.30	34.50	8.10	0	2.10	0
Yy3	1436.23 m	64.80	29.30	6.00	0	0	0
Yy3	1437.63 m	57.30	32.80	6.50	0	3.40	0
Yy3	1440.98 m	42.30	49.10	5.70	0	2.30	0.50
Yy3	1442.58 m	46.30	44.50	5.80	0	3.50	0
Yy3	1445.41 m	5.60	91.20	0.70	0	1.80	0.67
Yy3	1447.23 m	5.30	90.20	1.90	0	1.60	1.00
Yy3	1450.90 m	32.50	61.80	4.10	0	1.60	0
Yy3	1451.55 m	53.10	34.60	6.00	4.60	1.70	0
Yy3	1452.14 m	43.40	39.90	6.90	4.70	1.80	2.30
Yy2	2695.50 m	54.00	36.50	8.40	0	1.10	0
Yy2	2696.00 m	50.40	37.00	6.40	0	6.20	0
Yy2	2697.00 m	51.50	39.30	8.00	0	1.20	0
Yy2	2698.00 m	50.30	40.50	7.60	0	1.60	0
Yy2	2699.00 m	53.90	35.80	6.90	0	2.70	0.70
Yy2	2700.00 m	48.50	42.80	7.30	0	1.40	0
Yy2	2701.00 m	48.70	42.10	6.90	0	2.30	0
Yy2	2702.00 m	46.00	38.50	8.20	0	4.70	2.60
Yy2	2703.00 m	43.90	43.30	6.60	0	6.20	0
Yy2	2703.50 m	39.90	39.00	8.40	0	6.70	4.10
Yy2	2704.00 m	38.20	42.10	8.20	0	4.90	4.70
Yy2	2705.00 m	42.20	47.30	6.20	0	4.30	0
Yy2	2706.00 m	40.90	40.40	9.20	0	9.50	0
Yy2	2707.00 m	29.60	39.50	9.00	0	11.90	8.60
Yy2	2707.90 m	32.20	39.80	10.60	0	2.40	14.10
Yy2	2708.80 m	27.70	33.90	22.10	0	7.10	6.40
Yy2	2710.00 m	24.10	50.10	10.60	0	7.00	8.20
Yy2	2710.90 m	20.40	66.30	7.30	0	4.20	1.80
Yy2	2711.90 m	22.80	65.20	6.30	0	4.10	1.60
Yy2	2712.70 m	23.20	63.50	5.60	0	4.40	1.70
Yy2	2713.10 m	24.80	44.10	7.40	0	7.30	15.40
Yy2	2713.60 m	10.50	17.80	5.60	0	4.90	59.80
Yy2	2714.40 m	27.40	36.20	2.60	0	19.30	14.50
Yy2	2715.00 m	20.50	69.30	2.10	0	3.40	4.70
Yy2	2716.00 m	15.30	78.50	1.40	0	2.50	2.30
Yy2	2717.00 m	8.50	88.80	0.80	0	0	1.90
Yy2	2718.20 m	33.10	61.00	4.00	0.80	0.80	0.30
Yy2	2719.00 m	42.40	35.70	7.30	0	3.40	9.70
Hengshi	S_1l-1	29.70	42.50	6.10	5.80	0	8.10
Hengshi	S_1l-2	30.40	54.00	7.60	8.00	0	0
Hengshi	S_1l-3	22.00	67.80	5.40	4.70	0	0
Hengshi	S_1l-4	18.00	74.70	3.40	3.90	0	0
Hengshi	S_1l-5	13.00	77.20	5.10	4.70	0	0
Hengshi	S_1l-6	9.20	79.50	4.60	6.70	0	0
Hengshi	S_1l-7	11.70	76.60	3.00	8.70	0	0
Hengshi	S_1l-8	28.10	55.30	11.00	5.60	0	0
Hengshi	S_1l-9	19.00	62.90	14.70	3.40	0	0
Hengshi	S_1l-10	22.50	67.80	9.70	0	0	0
Hengshi	S_1l-11	20.90	68.80	10.30	0	0	0
Hengshi	S_1l-12	60.8	32.90	6.40	0	0	0
Hengshi	S_1l-13	81.10	8.10	8.90	0	2.00	0
Hengshi	S_1l-14	42.30	52.10	5.60	0	0	0
Hengshi	S_1l-15	42.60	52.20	5.20	0	0	0
Hengshi	S_1l-16	49.70	44.70	5.70	0	0	0
Hengshi	S_1l-17	85.10	10.90	4.00	0	0	0
Hengshi	S_1l-18	43.10	50.40	6.40	0	0	0
Hengshi	S_1l-19	65.10	30.00	4.90	0	0	0
Hengshi	S_1l-20	27.50	26.20	1.50	1.70	0	43.20

ranging from 0.21 to 3.14 (average of 0.99) and 1.07 to 14.18 (average of 3.44), respectively. Ni/Al ranged from 1.7×10^{-4} to 62.64×10^{-4} showing an upward decrease and P/Al ranged from 23.09×10^{-4} to 177.96×10^{-4}, which are considered as effective parameters for evaluating marine paleoproductivity (Lewan and Maynard, 1982; Poter et al., 2014; Khan et al., 2019).

The total rare earth element (ΣREE) content varied from 138.68 to 221.78 with an average of 189.63 (Table 3). The ratio of light rare earth element to heavy earth elements (LREE/HREE) ranged from 6.72 to 10.64 (average of 8.56). Eu/Eu* values exhibited significant negative anomalies and had an average value of 0.66 and the mean value of Ce/Ce* is 0.96 with a range of 0.91–0.96.

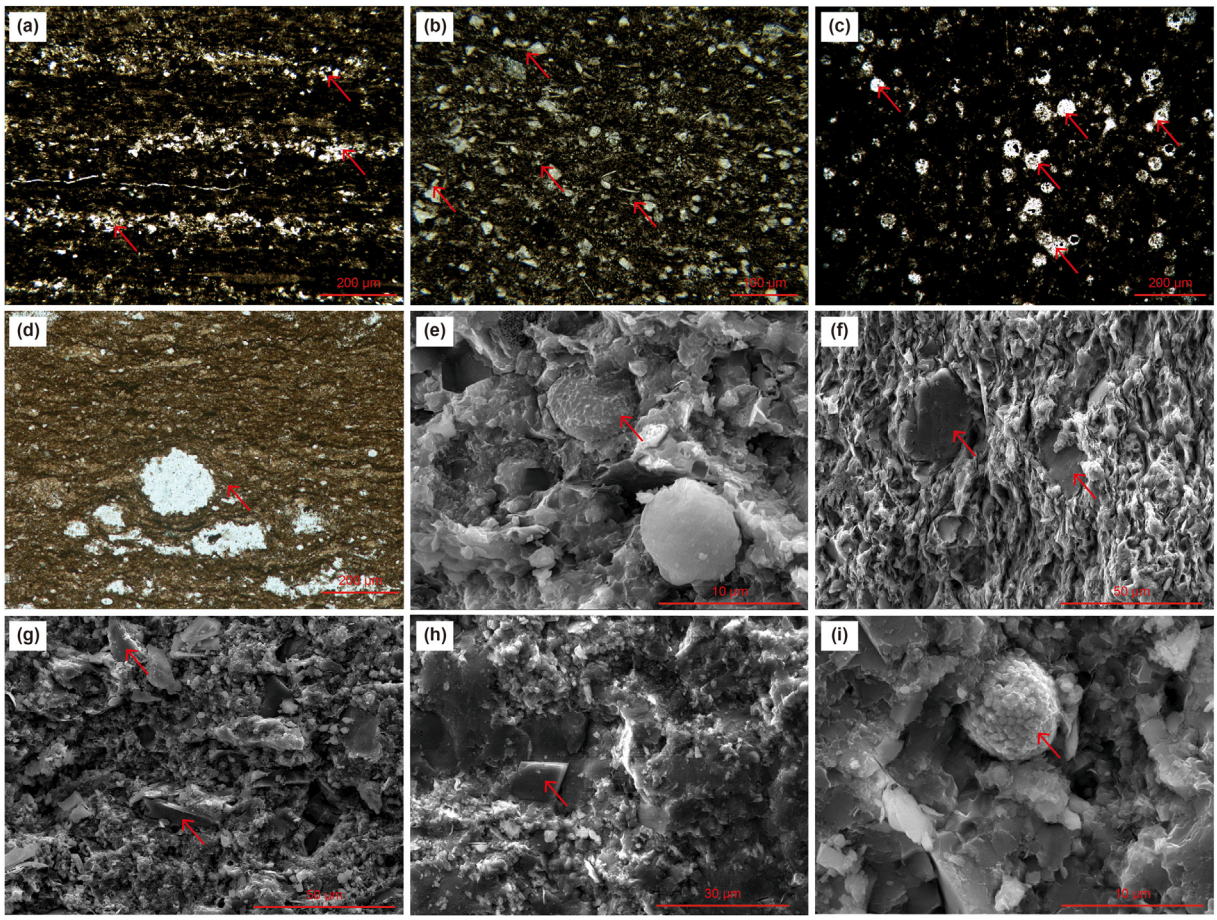

Fig. 3. Micrographs of minerals from the O_3w-S_1l black shale. (a) Terrigenous detrital quartz along lamina in S_1l black shale, Well Yy2; (b) Scattered detrital quartz in S_1l black shale, Well Yy2; (c) Massive siliceous radiolarians in O_3w black shale, Well Yy2; (d) Siliceous radiolarians and syn-sedimentary laminae in S_1l black shale, Hengshi section; (e) Siliceous radiolarian and its Si element content reaches 69% in S_1l black shale, Well Yy2; (f) Plagioclase, illite and mixed layer illite/smectite in S_1l black shale, Well Yy2; (g) K-feldspar in S_1l black shale, Well Yy2; (h) Ferrodolomite in S_1l black shale, Well Yy2; and (i) Pyrite framboid in O_3w black shale, Well Yy2. Arrows in each photo refer to corresponding minerals.

5. Discussion

5.1. Origin of silica

Biogenic, terrigenous detrital, and hydrothermal are the three primary sources for silica in marine deposits. Marine shale containing silica from different origins commonly has distinctive petrological, geochemical, and paleo-biological characteristics that can be used to identify silica sources (Adachi et al., 1986; Murray et al., 1994; Chen et al., 2006; Zhou et al., 2006; Harris et al., 2011; Qiu et al., 2018; Khan et al., 2019; Liu et al., 2019). Terrigenous silica, primarily from silicate and aluminosilicate minerals, has a close relationship with terrigenous input (Liu et al., 2017; Li et al., 2019). Detrital quartz is resistant to weathering and can be deposited after long-distance transport, and it is one of the primary forms of terrigenous silica in marine shale (Wright, 2001; Schieber, 2016; Zhao et al., 2016; Dong et al., 2019). Abundant terrigenous detrital quartz and feldspar are observed in the O_3w-S_1l black shale, and the detrital quartz usually has an angular shape with a diameter of 10–25 μm (Fig. 3a and b and 5i). Meanwhile, sandy layers are widely distributed in the S_1l black shale (Figs. 3a and 4), indicating that the terrigenous detrital source is an important origin of silica in the study area, which is consistent with widely developed sandy gravity flows in the upper Rhuddanian (Wang et al., 2015).

TiO_2 and Al_2O_3 are useful proxies for terrigenous input and the variations in their content can reflect the intensity of terrigenous silica influence on marine deposits (Milliken et al., 2016; Liu et al., 2017; Li et al., 2019). TiO_2 and Al_2O_3 concentrations show a long-term increasing upward trend in three studied sections, indicating the gradually increasing influence of terrigenous input (Fig. 7). However, the average TiO_2 and Al_2O_3 contents in the black shale are only 0.65% and 13.11%, which are less than that of PAAS (0.99% for TiO_2 and 15.9% for Al_2O_3) (Taylor and Mcclennans, 1985), showing a relatively minor influence of terrigenous input on black shale except shale during the Aeronian (Fig. 7). Significant negative correlations between SiO_2 versus TiO_2 and SiO_2 versus Al_2O_3 indicate that there are additional silica sources in the O_3w-S_1l black shale besides normal terrigenous silica deposits (Si_{excess} in section 2). Meanwhile, the Katian-Rhuddanian black shale with less TiO_2 and Al_2O_3 usually has higher SiO_2 content, indicating that the additional silica source makes an important contribution to the total silica (Fig. 7).

The ratios of Si/(Si + Al + Fe) and Al/(Al + Fe + Mn), and the Eu anomalies are effective parameters for identifying the origin of Si_{excess} in marine shale (Adachi et al., 1986; Yamamoto, 1987; Murray, 1994; Qiu et al. 2011, 2018; Zhang et al., 2018; Jiang et al., 2019; Khan et al., 2019; Li et al., 2019). Previous studies have shown that Si/(Si + AL + Fe) for biogenic silicalite is commonly higher than 0.90, Al/(Al + Fe + Mn) is higher than 0.6, and Eu anomalies are negative (Adachi et al., 1986; Yamamoto, 1987; Qiu et al., 2018; Khan et al., 2019; Li et al., 2019). For hydrothermal silicalite, Al/(Al + Fe + Mn) is less than 0.3, Eu anomalies are

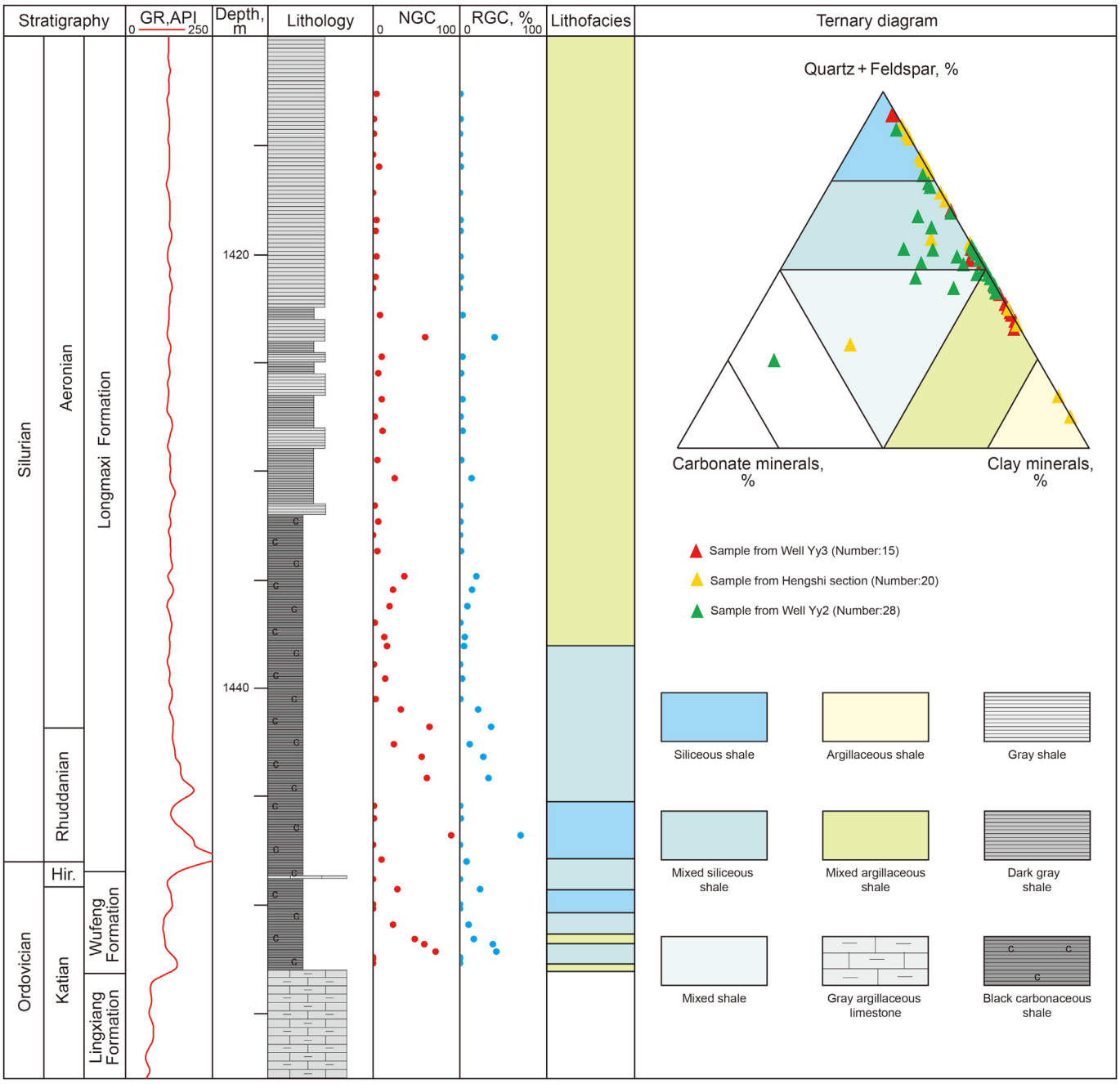

Fig. 4. Shale lithofacies of the O_3w-S_1l black shale and its vertical variations in Well Yy3. The ternary diagram is modified from Wang et al. (2019). Changes in graptolite abundance are marked as NGC and RGC. Hir = Hirnantian, NGC = number of graptolites on the core bedding surface, and RGC = ratio between total graptolite surface area and core bedding surface area.

positive, and shale with a lower Al/(Al + Fe + Mn) ratio and higher Eu/Eu* ratio generally reflect stronger hydrothermal activity (Adachi et al., 1986; Murray, 1994; Qiu et al., 2011; Zhang et al., 2018). In the study area, samples from the O_3w-S_1l black rock series have Si/(Si + Al + Fe) and Al/(Al + Fe + Mn) values ranging from 0.65 to 3.52 (averaging 1.17) and 0.39 to 0.85 (averaging 0.66) (Table 2), respectively, and the average Eu/Eu* value is 0.66 (Table 3). These results are most like the parameters for biogenic silicalite, indicating that Si_{excess} may be biogenic. Moreover, according to the Al–Fe–Mn ternary chart, the majority of samples plot in the bio-origin zone (Adachi et al., 1986) (Fig. 8). Therefore, we infer that the excess silica in the O_3w-S_1l black shale is biogenic rather than hydrothermal in origin. This inference coincides with the semi-restricted continental shelf environment of the O_3w-S_1l, where the average Ce/Ce* of samples is 0.96 (Table 3), greater than that of sediments at mid-oceanic ridges (averaging 0.3) and oceanic basins (with an average of 0.6) (Murrayet al.,1991; Murray, 1994).

Furthermore, the paleoproductivity and petrology also provide strong evidence for excess silica that are biogenic. High Si_{excess} content is primarily present in siliceous shale and mixed siliceous shale, while mixed argillaceous shale and argillaceous shale have little Si_{excess} content, and these features coincide with the numbers of observed siliceous organisms in different lithofacies (Fig. 3). In the O_3w-S_1l siliceous shale, siliceous radiolarians are widely

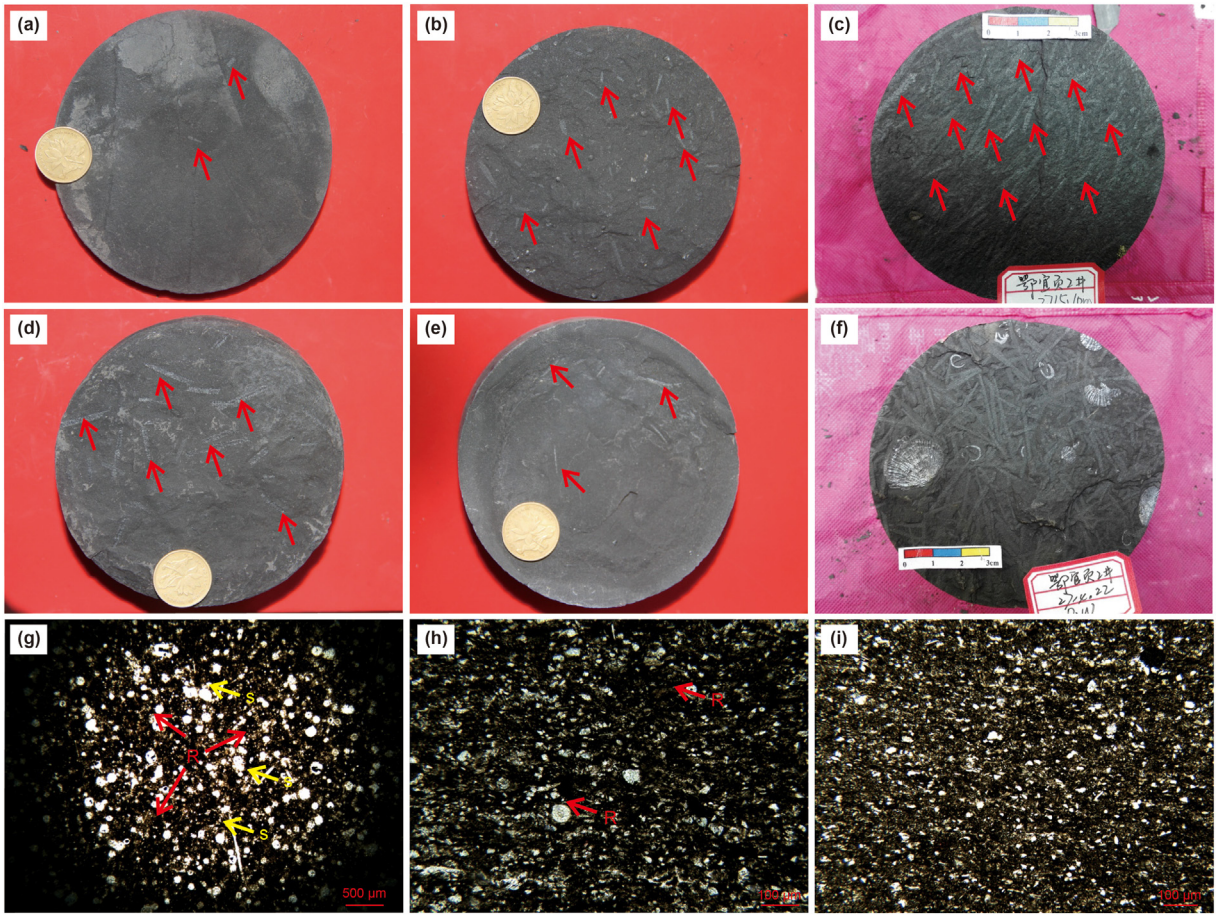

Fig. 5. Fossils in the O_3w-S_1l black shale. Arrows point to graptolites in (a) Siliceous shale; (b–d) Mixed siliceous shale; (e) Mixed argillaceous shale; (f) Hirnantia fauna and abundant graptolites in mixed siliceous shale; (g) Massive radiolarians and some sponge spicules in siliceous shale; (h) Several radiolarians in mixed siliceous shale; and (i) Mixed argillaceous shale without siliceous fossils. S = sponge spicule; R = radiolarian.

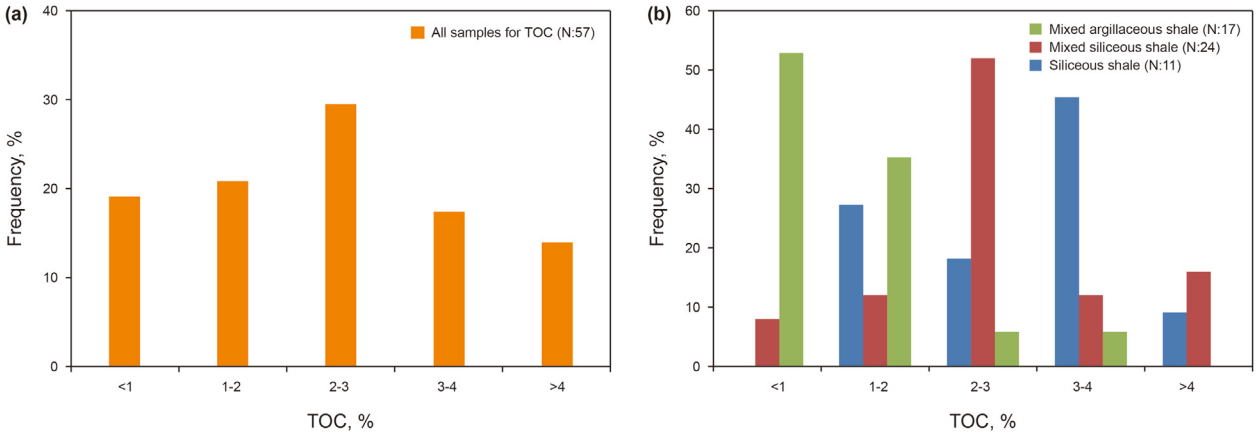

Fig. 6. (a) TOC histogram for the O_3w-S_1l black shale. (b) TOC histogram for different black shale lithofacies in the O_3w-S_1l black shale.

distributed (Figs. 3c and 5g), and few radiolarians are found in mixed argillaceous shale (Figs. 3a and 5i). Moreover, the Si_{excess} value shows good linear correlations with paleoproductivity proxies (Ni/Al and P/Al) except for some samples with higher Si_{excess} content (Fig. 9), indicating the O_3w-S_1l black shale Si_{excess} origin is biogenic (Bio-Si). Therefore, it can be concluded that Bio-Si and terrigenous siliciclastic input are the main O_3w-S_1l black shale silica sources.

5.2. Relationships between origins of silica and organic matter accumulation

Terrigenous detrital input has an important influence on marine organic matter accumulation (Murphy et al., 2000; Sageman et al., 2003; Li et al., 2017; Khan et al., 2019). Generally, high terrigenous influx will promote organic matter burial and diminish its exposure time while substantially diluting its abundance, resulting in lower

Table 2
Main geochemical parameters of the O_3w-S_1l black shale from Yy2 and Yy3 wells, and Hengshi Section.

Section name	Sample location	SiO_2, %	Al_2O_3, %	TiO_2, %	Fe_2O_3, %	FeO, %	CaO, %	K_2O, %	Na_2O, %	P_2O_5, %	MnO_2, %	U, ppm	Th, ppm	V, ppm	Cr, ppm	Ni, ppm	Si_{excess}, %	U/Th	V/Cr	Ni/Al, $\times 10^{-4}$	P/Al, $\times 10^{-4}$	Al/Ti, $\times 10^{-2}$	Si/(Si + Al + Fe)	Al/(Al + Fe + Mn)	CIA	TOC, %
Yy3	1413.76 m	59.82	18.40	0.71	1.77	4.76	0.30	4.52	1.13	0.10	0.05	3.64	17.10	135.00	112.00	61.10	0.00	0.21	1.21	6.27	45.72	22.58	0.66	0.66	76.51	0.77
Yy3	1415.40 m	60.97	17.97	0.75	1.43	5.05	0.29	4.34	1.20	0.11	0.06	3.46	16.50	120.00	110.00	48.20	0.00	0.21	1.09	5.07	51.86	21.02	0.66	0.66	76.44	0.36
Yy3	1417.16 m	60.75	17.77	0.75	2.21	4.49	0.29	4.28	1.17	0.12	0.06	2.62	11.30	138.00	102.00	49.40	0.00	0.23	1.35	5.25	54.30	20.74	0.66	0.65	76.53	–
Yy3	1418.91 m	59.74	17.83	0.75	1.55	5.22	0.36	4.33	1.19	0.11	0.05	3.92	18.40	118.00	115.00	66.30	0.00	0.21	1.03	7.02	50.88	20.94	0.66	0.65	76.36	1.11
Yy3	1422.80 m	59.18	17.64	0.79	0.84	5.61	0.58	4.29	1.16	0.10	0.06	5.45	18.90	149.00	109.00	67.40	0.00	0.29	1.37	7.22	48.62	19.54	0.66	0.65	75.65	1.39
Yy3	1428.14 m	59.05	17.50	0.76	2.63	4.06	0.50	4.33	1.10	0.10	0.06	3.87	13.80	179.00	106.00	84.20	0.00	0.28	1.69	9.09	48.07	20.07	0.66	0.65	75.78	–
Yy3	1432.31 m	59.83	16.98	0.72	2.69	3.80	0.71	4.22	1.10	0.10	0.06	4.76	16.20	150.00	98.00	70.10	0.00	0.29	1.53	7.80	48.57	20.52	0.67	0.65	74.88	1.70
Yy3	1432.95 m	62.80	16.66	0.68	1.27	4.97	0.33	4.00	1.16	0.12	0.05	4.41	16.50	112.00	97.80	40.80	1.88	0.27	1.15	4.63	58.91	21.32	0.71	0.65	76.35	0.44
Yy3	1434.84 m	61.91	16.06	0.77	1.60	4.73	0.40	3.98	1.10	0.10	0.05	5.37	15.20	104.00	92.60	63.10	2.45	0.35	1.12	7.42	52.89	18.23	0.73	0.64	75.76	1.23
Yy3	1436.23 m	62.25	16.41	0.70	1.67	4.26	0.49	4.14	1.03	0.11	0.05	3.95	15.10	192.00	98.70	66.40	2.03	0.26	1.95	7.64	52.77	20.40	0.72	0.66	75.56	1.27
Yy3	1437.63 m	60.92	15.65	0.73	6.09	1.41	0.51	3.86	1.08	0.11	0.05	5.78	14.80	130.00	93.10	83.20	2.66	0.39	1.40	10.04	56.39	18.79	0.72	0.61	75.45	1.83
Yy3	1442.58 m	64.33	13.90	0.62	2.08	4.22	0.59	3.43	1.00	0.11	0.04	6.60	12.90	111.00	75.40	68.10	7.13	0.51	1.47	9.25	65.86	19.68	0.86	0.61	74.92	2.24
Yy3	1445.41 m	82.56	4.31	0.30	0.76	1.80	1.16	0.93	0.62	0.09	0.03	9.92	6.34	86.40	33.80	66.10	31.43	1.56	2.56	28.97	177.96	12.66	3.41	0.54	66.57	3.72
Yy3	1446.78 m	67.03	8.09	0.51	5.09	1.98	3.79	1.81	1.06	0.14	0.06	50.10	14.70	219.00	43.60	184.00	17.96	3.41	5.02	42.96	139.66	13.83	1.38	0.45	67.30	4.40
Yy3	1447.23 m	84.70	3.75	0.25	1.37	2.71	0.79	0.82	0.53	0.06	0.04	15.50	5.81	112.00	39.90	70.40	33.35	2.67	2.81	35.46	123.16	13.23	3.52	0.39	66.68	1.28
Yy3	1451.55 m	69.28	12.93	0.54	0.29	3.52	0.44	3.58	0.77	0.10	0.03	4.08	14.50	105.00	72.70	49.20	11.04	0.28	1.44	7.19	61.23	20.80	1.04	0.70	74.34	3.32
Yy3	1452.14 m	59.66	14.93	0.94	0.13	4.60	0.96	4.12	0.99	0.16	0.04	4.95	14.60	368.00	145.00	86.30	3.26	0.34	2.54	10.92	87.28	13.89	0.77	0.68	72.95	4.16
YY2	2695.50 m	60.02	17.96	0.71	2.61	3.49	0.34	4.44	1.08	0.11	0.06	2.17	5.10	133.00	85.80	44.90	0.00	0.43	1.55	4.72	48.68	22.11	0.67	0.67	76.49	0.38
Yy2	2696.00 m	62.02	17.10	0.74	2.55	3.85	0.32	4.18	1.11	0.11	0.05	3.26	6.19	126.00	88.60	49.40	0.79	0.53	1.42	5.46	54.02	20.36	0.69	0.65	76.37	0.61
YY2	2697.00 m	63.06	16.88	0.75	4.55	1.18	0.42	4.22	1.11	0.11	0.05	3.66	10.20	130.00	78.00	47.40	1.64	0.36	1.67	5.30	54.23	19.64	0.72	0.68	75.83	0.66
YY2	2698.00 m	62.48	17.05	0.72	4.47	1.90	0.28	4.22	1.10	0.11	0.05	3.54	8.48	172.00	90.60	54.90	1.09	0.42	1.90	6.08	52.72	20.70	0.70	0.66	76.22	0.68
YY2	2699.00 m	61.48	17.70	0.73	4.65	1.91	0.27	4.35	1.06	0.11	0.05	2.81	8.49	126.00	88.90	43.50	0.00	0.33	1.42	4.64	51.72	21.10	0.67	0.66	76.59	0.44
YY2	2700.00 m	61.74	16.92	0.75	4.11	2.46	0.35	4.12	1.13	0.11	0.05	3.56	7.16	156.00	91.60	68.10	0.95	0.50	1.70	7.60	54.59	19.72	0.69	0.65	76.32	0.99
YY2	2701.00 m	60.20	16.02	0.74	3.28	3.68	1.04	3.92	1.14	0.11	0.08	5.45	7.94	142.00	76.20	57.60	1.72	0.69	1.86	6.79	56.63	19.05	0.70	0.62	73.64	0.98
YY2	2702.00 m	61.61	15.25	0.73	4.92	1.81	0.96	3.65	1.15	0.11	0.07	6.11	8.35	118.00	73.10	61.10	3.64	0.73	1.61	7.57	59.49	18.28	0.76	0.62	73.86	1.39
YY2	2703.00 m	61.45	15.24	0.69	5.45	1.72	0.62	3.70	1.04	0.12	0.04	5.92	7.00	131.00	79.40	53.10	3.58	0.85	1.65	6.58	63.32	19.33	0.75	0.61	75.39	2.24
YY2	2703.50 m	62.30	15.32	0.69	5.72	0.95	0.51	3.82	1.01	0.10	0.04	5.28	4.94	182.00	79.50	96.30	3.85	1.07	2.29	11.87	55.99	19.35	0.76	0.63	75.41	2.04
YY2	2704.00 m	60.36	14.51	0.76	6.49	1.09	0.84	3.63	0.95	0.10	0.04	6.57	5.53	144.00	75.80	99.70	4.28	1.19	1.90	12.98	59.11	16.66	0.76	0.59	74.09	2.37
YY2	2705.00 m	64.46	13.74	0.61	2.68	3.94	0.53	3.40	0.91	0.10	0.03	6.43	5.90	131.00	69.80	86.80	7.46	1.09	1.88	11.93	60.62	19.65	0.86	0.59	75.34	2.02
YY2	2706.00 m	60.98	14.56	0.69	5.38	1.86	0.78	3.53	1.16	0.11	0.04	8.48	8.33	128.00	73.80	88.70	4.48	1.02	1.73	11.51	62.31	18.52	0.77	0.60	74.04	2.62
YY2	2707.00 m	59.23	14.27	0.70	6.84	0.76	0.66	3.55	1.09	0.12	0.03	20.90	8.95	117.00	67.60	64.10	4.15	2.34	1.73	8.48	67.04	17.82	0.76	0.58	74.37	2.92
YY2	2707.90 m	60.90	17.94	0.61	4.56	0.58	0.79	4.14	1.54	0.13	0.03	14.10	16.70	82.90	39.00	58.80	0.00	0.84	2.13	6.19	58.38	25.74	0.68	0.72	74.79	1.76
YY2	2708.80 m	68.95	11.49	0.65	1.53	2.35	2.20	2.36	1.67	0.13	0.04	15.00	17.50	199.00	54.20	92.70	13.26	0.86	3.67	15.24	92.59	15.45	1.15	0.68	66.84	2.17
YY2	2710.00 m	69.86	9.84	0.58	2.96	1.80	2.31	2.14	1.28	0.11	0.05	16.40	15.40	140.00	50.60	102.00	16.40	1.06	2.77	19.58	93.87	14.95	1.31	0.60	67.68	2.45
YY2	2710.90 m	65.40	12.69	0.85	3.31	1.75	0.75	3.05	1.04	0.12	0.03	13.40	11.40	560.00	59.90	145.00	9.63	1.18	9.35	21.58	77.34	13.10	0.98	0.64	74.07	3.85
YY2	2711.90 m	76.20	7.30	0.43	1.72	1.26	1.63	1.66	0.73	0.08	0.02	11.20	8.06	387.00	38.60	120.00	23.54	1.39	10.03	31.05	88.12	14.82	1.97	0.64	70.06	3.78
YY2	2712.70 m	68.02	9.20	0.56	3.17	1.54	2.21	2.15	1.09	0.11	0.03	25.20	11.20	595.00	66.30	182.00	16.60	2.25	8.97	37.37	96.82	14.33	1.35	0.59	68.00	5.37
YY2	2713.10 m	69.79	9.19	0.56	2.27	1.33	1.40	2.17	1.05	0.10	0.03	27.60	10.10	714.00	70.70	167.00	17.44	2.73	10.10	34.32	92.43	14.39	1.44	0.65	68.28	5.30
YY2	2713.60 m	63.60	11.58	0.53	3.61	1.46	2.04	2.81	1.20	0.13	0.04	27.20	14.50	764.00	58.50	162.00	10.61	1.88	13.06	26.42	89.74	19.05	1.03	0.62	68.97	5.53
YY2	2714.40 m	64.35	9.83	0.57	4.12	1.31	2.85	2.51	0.99	0.13	0.04	23.20	12.10	250.00	59.90	123.00	13.85	1.92	4.17	23.64	104.87	15.07	1.19	0.57	68.65	5.52
YY2	2715.00 m	68.20	7.91	0.43	2.05	2.38	4.01	1.99	0.67	0.08	0.14	9.57	10.50	298.00	62.80	82.60	18.80	0.91	4.75	19.72	87.58	16.06	1.55	0.55	70.39	2.58
YY2	2716.00 m	74.49	8.33	0.47	2.10	1.47	0.71	2.14	0.70	0.09	0.03	17.40	8.26	947.00	66.80	123.00	21.05	2.11	14.18	27.89	91.09	15.38	1.68	0.63	71.93	4.30
YY2	2717.00 m	83.61	4.74	0.27	0.97	2.19	0.87	1.24	0.40	0.06	0.03	8.72	8.57	423.00	50.10	66.20	31.21	1.02	8.44	26.38	97.44	15.48	3.07	0.51	69.85	2.55
YY2	2718.20 m	69.06	13.28	0.54	1.33	1.54	1.22	3.72	0.58	0.06	0.03	4.67	13.50	246.00	54.70	52.00	10.36	0.35	4.50	7.40	38.50	21.72	1.04	0.77	73.16	2.68
YY2	2719.00 m	58.39	17.46	0.85	3.79	2.06	0.33	5.00	0.79	0.09	0.08	2.92	8.52	222.00	68.50	48.60	0.00	0.34	3.24	5.26	43.46	17.93	0.67	0.68	75.00	3.01
Hengshi	S_1l-1	66.66	14.50	0.70	0.50	1.61	0.21	3.58	0.86	0.17	0.01	22.10	13.80	681.00	96.20	126.00	7.23	1.60	7.08	16.41	96.69	18.13	0.94	0.83	76.55	3.74
Hengshi	S_1l-2	73.46	9.13	0.56	0.65	0.86	0.18	2.80	0.68	0.06	0.01	25.80	10.10	885.00	79.40	87.80	19.25	2.55	11.15	18.16	56.01	14.32	1.63	0.81	72.43	6.38
Hengshi	S_1l-3	79.92	7.58	0.52	0.40	0.55	0.11	2.29	0.43	0.05	0.01	19.70	10.10	382.00	56.20	43.00	24.82	1.95	6.80	10.72	50.05	12.76	2.17	0.85	73.57	3.84
Hengshi	S_1l-4	76.39	7.69	0.68	0.46	0.56	0.14	2.16	0.70	0.03	0.01	44.40	13.40	211.00	43.80	255.00	22.99	3.31	4.82	62.64	35.39	9.85	2.04	0.84	72.65	2.95
Hengshi	S_1l-5	78.49	7.72	0.54	1.32	0.70	0.16	2.30	0.62	0.06	0.01	13.60	9.40	144.00	49.00	26.90	23.92	1.45	2.94	6.58	58.76	12.47	2.01	0.73	72.58	3.76
Hengshi	S_1l-6	80.97	6.95	0.51	0.21	1.04	0.20	2.07	0.64	0.04	0.01	9.09	8.45	150.00	48.30	23.60	26.34	1.08	3.11	6.41	47.47	11.97	2.35	0.79	71.53	3.90
Hengshi	S_1l-7	80.58	7.02	0.47	1.73	1.38	0.15	1.92	0.74	0.08	0.01	10.40	9.67	155.00	45.70	76.50	26.05	1.08	3.39	20.58	97.51	12.96	2.14	0.62	72.51	3.15
Hengshi	S_1l-8	71.19	13.93	0.77	0.97	1.08	0.56	3.69	1.34	0.04	0.01	8.89	16.60	130.00	73.50	30.40	10.29	0.54	1.77	4.12	23.09	15.81	1.04	0.83	71.86	1.78
Hengshi	S_1l-10	77.09	10.13	0.60	0.27	2.29	0.27	2.53	1.21	0.05	0.01	9.60	14.80	90.90	57.80	36.80	19.30	0.65	1.57	6.86	42.34	14.70	1.50	0.73	72.54	1.92
Hengshi	S_1l-12	76.70	10.04	0.61	0.64	2.03	0.18	2.46	1.16	0.07	0.02	8.14	13.10	104.00	59.60	21.10	19.26	0.62	1.74	3.97	56.68	14.50	1.50	0.72	73.50	2.26

Hengshi	S_1l-13	75.90	9.62	0.82	0.97	1.76	0.15	2.46	1.04	0.06	0.01	8.04	9.91	92.80	51.70	27.00	19.58	0.81	1.79	5.30	49.72	10.30	1.54	0.71		73.32	1.99
Hengshi	S_1l-15	69.34	13.35	0.89	1.40	1.08	0.30	3.76	0.88	0.05	0.01	7.67	12.20	133.00	76.00	12.00	10.38	0.63	1.75	1.70	31.51	13.10	1.05	0.79		73.67	2.41
Hengshi	S_1l-16	68.72	14.09	0.73	2.91	0.99	0.18	3.92	0.69	0.06	0.01	8.80	14.80	151.00	80.80	13.40	8.87	0.59	1.87	1.80	33.95	16.91	0.96	0.73		75.34	2.01
Hengshi	S_1l-17	62.95	17.02	0.76	4.59	1.80	0.35	4.04	0.89	0.11	0.03	3.18	14.20	110.00	104.00	42.60	1.35	0.22	1.06	4.73	53.30	19.55	0.71	0.66		77.54	–
Hengshi	S_1l-19	60.25	17.99	0.72	3.79	3.05	0.25	4.42	0.95	0.10	0.05	3.90	15.80	135.00	99.40	60.30	0.00	0.25	1.36	6.33	44.47	21.84	0.66	0.65		77.00	0.80

TOC values in marine shales with abundant terrigenous materials (Ibach, 1980; Rimmer, 2004; Lu et al., 2019; Wang et al., 2019). Hence, terrigenous detritus input is generally considered a negative factor for organic matter accumulation.

In marine black shale, Al_2O_3 is a direct proxy for terrigenous siliciclastic input, and the CIA can also help in analyzing the provenance weathering intensity of marine siliciclastic sediments (Milliken et al., 2016; Liu et al., 2017; Li et al., 2019; Wang et al., 2019). Despite the long-term increasing upward trend of CIA and Al_2O_3 in the O_3w-S_1l shale within the study area, indicating gradually increasing terrigenous detritus input and weathering intensity, the CIA value and Al_2O_3 content of samples show complex correlations with TOC (Fig. 10). CIA values > 73 have strong negative correlations with TOC, showing that weak weathering conditions may favor organic matter enrichment, but the negative correlations abruptly deteriorate when the CIA value is < 73, indicating that weak weathering conditions may not always be beneficial for organic matter accumulation (Fig. 10a). The Al_2O_3 and TOC contents exhibit a similar relationship (Fig. 10); Al_2O_3 content in black shale >12% has a strong negative correlation with TOC, indicating less terrigenous siliciclastic input will benefit the organic matter accumulation. However, it should be noted that the correlation is poor when the Al_2O_3 content is <12%, and Al_2O_3 content <8% shows a positive correlation with TOC, indicating that too little or too much terrigenous siliciclastic input are not favorable for the organic matter enrichment either. Sufficient terrigenous detrital supply will benefit organic matter preservation by diminishing exposure time, but it will substantially dilute organic matter abundance (Murphy et al., 2000; Sageman et al., 2003; Rimmer, 2004; Khan et al., 2019; Li et al., 2019; Lu et al., 2019). Too little terrigenous input will lead to the decrease in aluminosilicates, which function as effective organic matter absorbents (Rimmer, 2004), and the lack of aluminosilicates will slow organic matter burial rate and lead to widespread oxidation of organic matter in the water column (Ibach, 1980; Wang et al., 2019), resulting in low TOC in the black shale. Consequently, we infer that a certain amount of terrigenous siliciclastic input and appropriate weathering conditions should be most favorable for the organic matter accumulation in marine black shale. In other words, too much or too little terrigenous silica input will negatively influence marine organic matter enrichment.

In previous researches, Bio-Si content was regarded as an important paleoproductivity proxy, and linear relationships were usually utilized to describe the correlations between TOC and Bio-Si (Dong et al., 2019; Li et al., 2019; Lu et al., 2019; Khan et al., 2019). However, Bio-Si content (equal to Si_{excess}) and TOC of samples from the O_3w-S_1l black shale in the study area exhibit complex relationships (Fig. 11a and b). Black shale samples with 10%–20% Bio-Si contents usually have the maximum TOC. Furthermore, the Bio-Si contents show strong positive linear correlations with TOC when Bio-Si content remains below a certain threshold value (10%), and negative correlations to some extent when Bio-Si content exceeds 20% (Fig. 11a). These correlation characteristics are also consistent with published data (Dong et al., 2019; Khan et al., 2019; Liu et al., 2019). For example, although Khan et al. (2019) used a positive linear correlation to describe the relationship between TOC and Bio-SiO_2, it can be found that the relationship between TOC and Bio-SiO_2 is not linear; TOC in black shale gradually decreases with the increase in Bio-SiO_2 content when the Bio-SiO_2 content in black shale is greater than approximately 40% (equivalent to 18.6% of Bio-Si content) (Fig. 11b). The relationship between Bio-Si and TOC is also consistent with the variations in graptolite abundance in different lithofacies. Graptolites, as a kind of organic matter (Luo et al., 2016), are rare in siliceous shale and argillaceous shale (Fig. 5a, e), but are easily found in mixed siliceous shale (Fig. 5c).

Table 3
REE concentrations (ppm) and selected parameters of the O_3w-S_1l black shale from Well Yy2.

Sample depth, m	2696.00	2698.00	2701.00	2704.00	2707.90	2710.00	2713.10	2716.00	2719.00	Chondrite
La	44.20	45.60	41.20	39.20	43.30	38.50	32.60	28.20	51.50	0.38
Ce	89.00	91.60	85.00	80.40	86.30	78.00	64.40	54.00	91.80	0.98
Pr	9.63	9.77	9.32	8.88	8.97	8.67	7.60	6.53	9.59	0.14
Nd	35.70	35.50	35.40	33.30	32.20	32.80	30.40	25.70	35.10	0.72
Sm	6.44	6.19	6.88	6.20	5.96	6.21	6.08	5.17	6.73	0.23
Eu	1.34	1.14	1.54	1.38	1.24	1.16	1.32	1.11	1.41	0.09
Gd	5.70	5.29	5.98	5.38	5.61	5.59	5.58	4.78	6.47	0.31
Tb	0.86	0.78	0.92	0.81	0.90	0.88	0.89	0.79	1.10	0.06
Dy	4.97	4.51	5.25	4.71	5.60	5.18	5.31	4.77	7.03	0.39
Ho	1.00	0.92	1.06	0.96	1.17	1.04	1.08	1.01	1.47	0.09
Er	2.75	2.63	2.90	2.64	3.32	2.94	2.92	2.77	4.04	0.26
Tm	0.44	0.43	0.46	0.42	0.57	0.46	0.46	0.45	0.65	0.04
Yb	2.96	2.87	3.07	2.77	3.85	3.01	2.96	2.98	4.28	0.25
Lu	0.41	0.40	0.44	0.39	0.55	0.42	0.40	0.42	0.61	0.04
ΣREE	205.40	207.63	199.42	187.44	199.54	184.86	162.00	138.68	221.78	
LREE/HREE	9.76	10.64	8.93	9.37	8.25	8.47	7.27	6.72	7.65	
Eu/Eu*	0.67	0.60	0.73	0.72	0.65	0.60	0.69	0.68	0.65	
Ce/Ce*	0.98	0.98	0.99	0.98	0.98	0.97	0.93	0.91	0.92	

The value of Eu/Eu* and Ce/Ce* are calculated by the formula: $Eu/Eu^* = 2Eu_N/(Sm_N + Gd_N)$; $Ce/Ce^* = 2Ce_N/(La_N + Pr_N)$. The value of X_N is the concentration of element X normalized by chondrite.

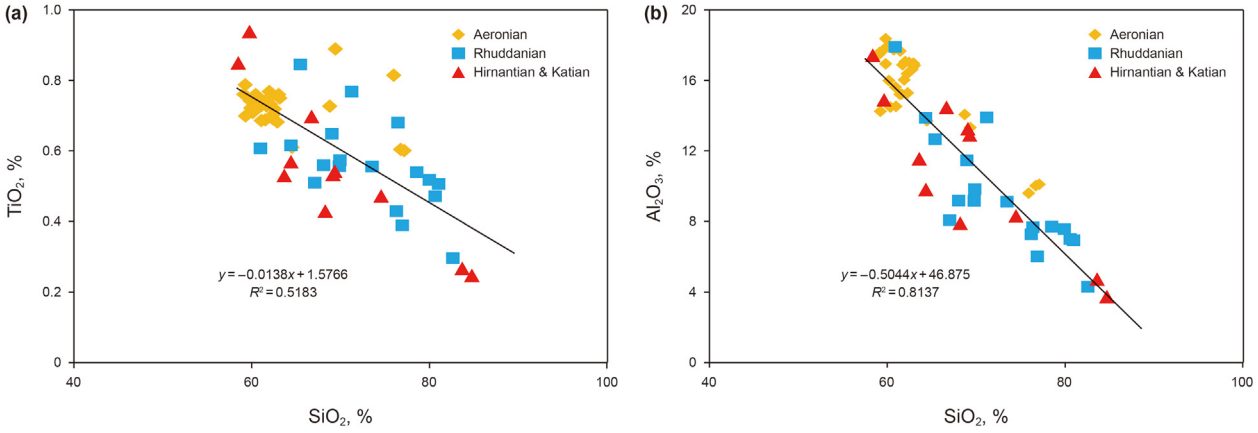

Fig. 7. Cross-plots of SiO_2 versus TiO_2 and Al_2O_3 of shale samples from the O_3w-S_1l black shale showing strong negative correlations.

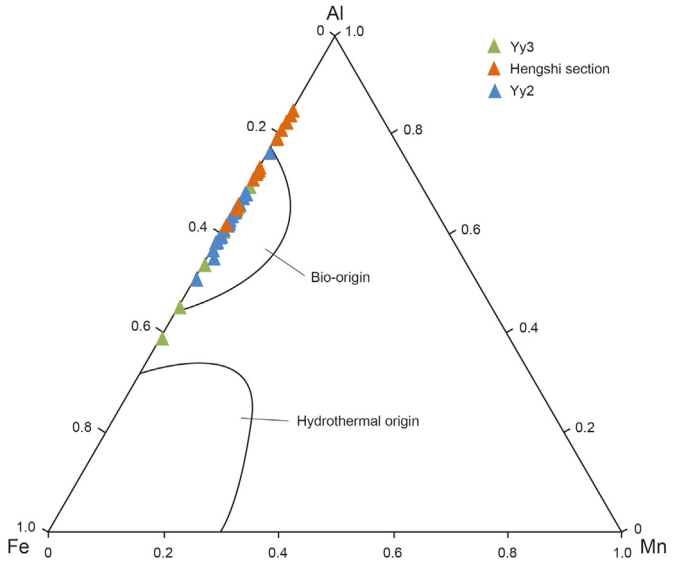

Fig. 8. Al–Fe–Mn ternary plot showing the siliceous origin of shale samples from the O_3w-S_1l black shale (Base map is modified from Adachi et al., 1986).

Therefore, it can be found that the O_3W–S_1l black shale with a specific content of Bio-Si or terrigenous siliciclastic input will have higher TOC values (Figs. 10 and 11), not the black shale with the highest Bio-Si content or the least terrigenous silica input. The relationship between graptolite abundance and silica from different origins can also illustrate the nonlinear correlations described above, in which shale with higher or lower Bio-Si content and terrigenous siliciclastic input reflected by Al_2O_3 usually have low graptolite abundance (Figs. 4, 5 and 12). Hence, a black shale with too much or too little Bio-Si content or terrigenous silica input indicates that there may be a decrease in TOC and graptolite abundance. These features also demonstrate that siliceous organisms with some hydrocarbon generation materials are not the primary organic source in the O_3w-S_1l black shale and using Bio-Si content to evaluate the organic matter enrichment of siliceous shale should, therefore, be evaluated carefully.

5.3. Sedimentary model for siliceous materials and organic matter

Based on the above geochemical and petrological analysis, terrigenous siliciclastic input and Bio-Si constitute the main sources of silica in the O_3w-S_1l black shale (Fig. 13). In the Well Yy2

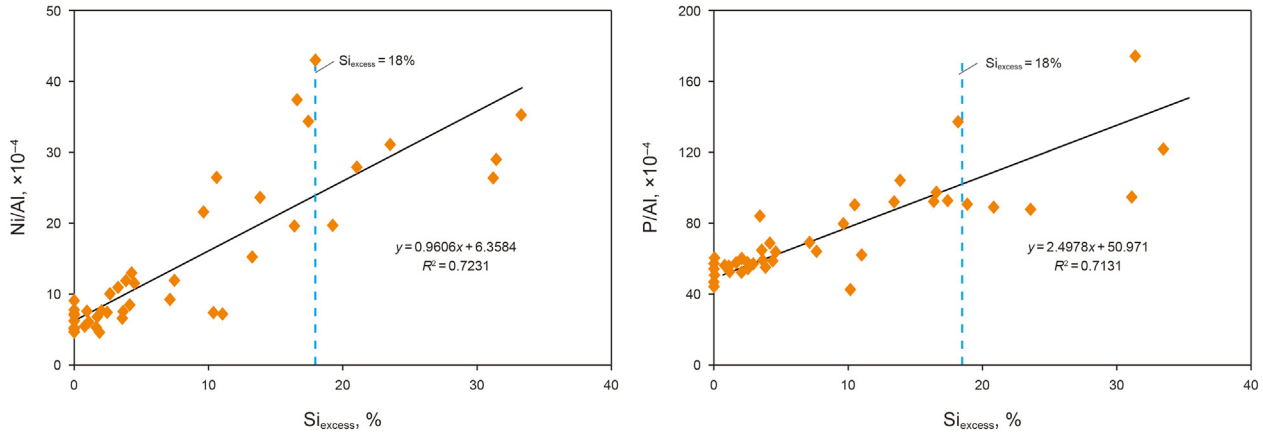

Fig. 9. Cross plots of Ni/Al and P/Al versus Si_{excess} for shale samples from the O_3w-S_1l black shale in wells Yy3 and Yy2.

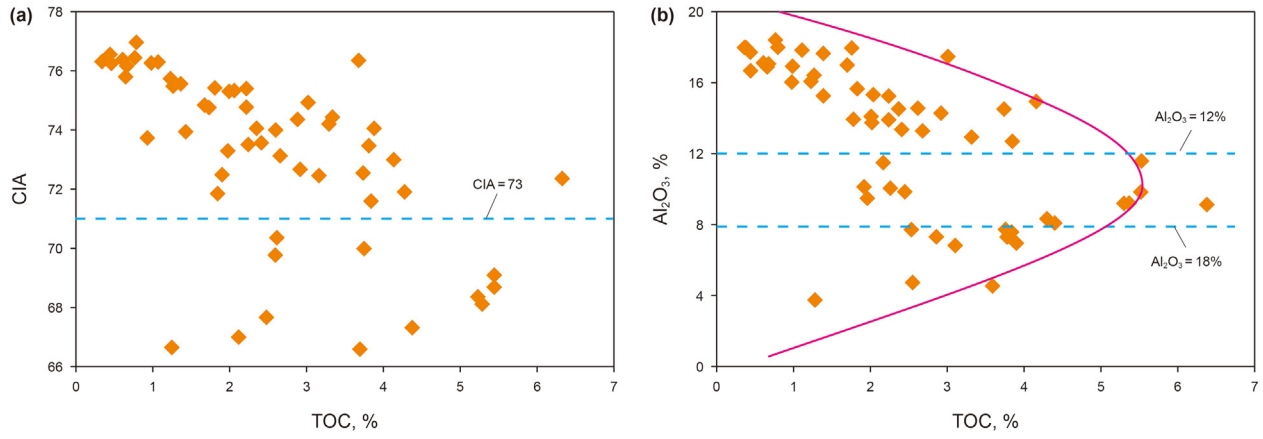

Fig. 10. Cross-plots of TOC versus CIA and Al_2O_3 of the O_3w-S_1l shale samples showing a complex correlation between terrigenous siliciclastic input and organic matter enrichment.

profile, the normal terrigenous siliciclastic deposits represented by Al_2O_3 show a long-term increasing trend, whereas the Bio-Si content decreases upward. Meanwhile, the geochemical proxies such as U/Th and V/Cr exhibit a long-term decreasing trend and CIA values show gradual increase, indicating a gradually oxidizing environment with sea-level fall and an intensifying weathering condition during the depositional stage of the O_3w-S_1l black shale (Fig. 13). Shale samples with high Bio-Si and TOC contents only occur in the O_3W and the lower S_1l, in which the U/Th and V/Cr ratios are higher than 0.75 and 2, respectively (Fig. 13). These variations in geochemical proxies indicate that Bio-Si prefers reducing environments and terrigenous silica prefers oxidizing environments, and a strong reducing environment with relatively high sea level and productivity may be beneficial for organic matter accumulation (Liu et al. 2016, 2019; Dong et al., 2018; Zhang et al. 2018, 2019; Lu et al., 2019; Yan et al., 2019).

However, the cross-plots of TOC versus V/Cr and U/Th in the O_3w-S_1l black shale exhibit nonlinear correlations rather than a simple linear relationship when the V/Cr and U/Th ratios are >5.0 and 2.0, respectively (Fig. 14). Meanwhile, graptolites are rare in siliceous shale formed in a strongly reducing environment and argillaceous shale formed in an oxidizing environment (Fig. 5a, e), but are very common in mixed siliceous shale formed in a relatively reducing environment (Fig. 5c). These characteristics indicate that an appropriate redox condition should be more favorable for organic matter accumulation, rather than the strongest reducing environment.

Organic matter enrichment is primarily controlled by the supply and preservation of organisms. The supply of organisms is closely related to paleoproductivity, and organic matter preservation primarily depends on redox conditions, burial rate, and hydrodynamic conditions (Murphy et al., 2000; Sageman et al., 2003; Li et al. 2017, 2019; Lu et al., 2019; Khan et al., 2019; Yang et al., 2019). According to the above nonlinear relationships of TOC versus silica origin and redox parameters, the O_3w-S_1l shale is taken as an example to establish a sedimentary model for organic matter and silica origin distribution within a continental shelf with little hydrothermal influence.

During the Ordovician-Silurian transition, the Yangtze area was a semi-restricted shelf covered by a broad epeiric sea (Chen et al., 2004; Su et al., 2009; Gorjan et al., 2012; Liu et al., 2017). With the early sea-level rise, an upwelling current provided plentiful nutrients to the semi-enclosed shelf basin, leading to an increase in marine primary productivity and in Bio-Si content characterized by abundant siliceous radiolarians (Figs. 13 and 15). Many planktonic organisms, including graptolites, are well-preserved in deep-water sediments (Figs. 4 and 5), resulting from gradually strengthening anoxic conditions and a weakening hydrodynamic environment (Figs. 4 and 13). However, seawater nutrients cannot increase continuously and even decrease when the rising sea level exceeds a certain limit, just like the lack of nutrients in the modern ocean (Platt and Sathyendranath, 1988; Li et al., 2003). Siliceous radiolarians are more common with continuously rising sea level (Khan et al., 2019), while enhanced open seawater environments lead to the migration

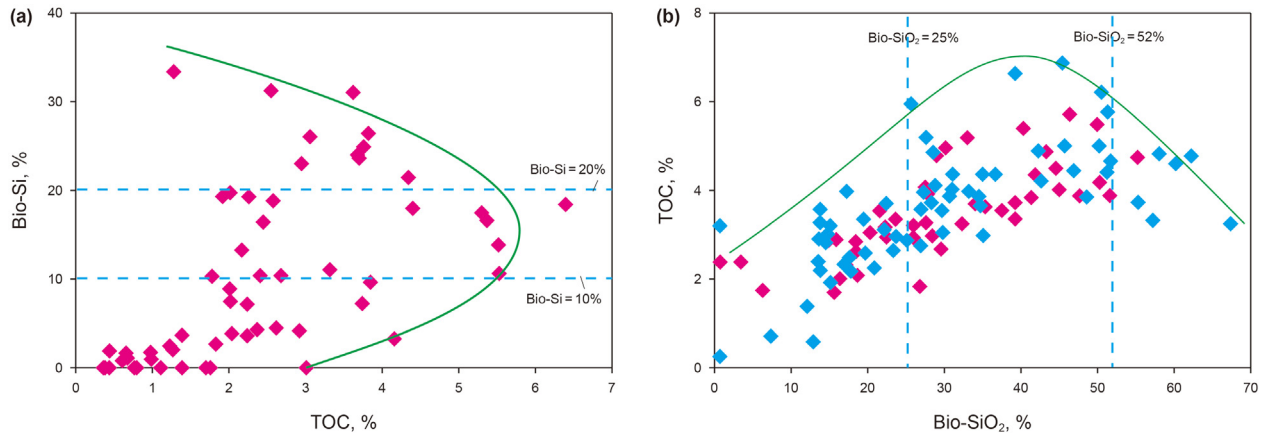

Fig. 11. Complex correlation between TOC versus Bio-Si and Bio-SiO_2 content. (a) Cross plot of Bio-Si content versus TOC for the O_3w-S_1l black shale samples in the study area. (b) Cross plot of Bio-SiO_2 content versus TOC for the O_3w-S_1l black shale samples in Sichuan Basin, and data are taken from Khan et al. (2019).

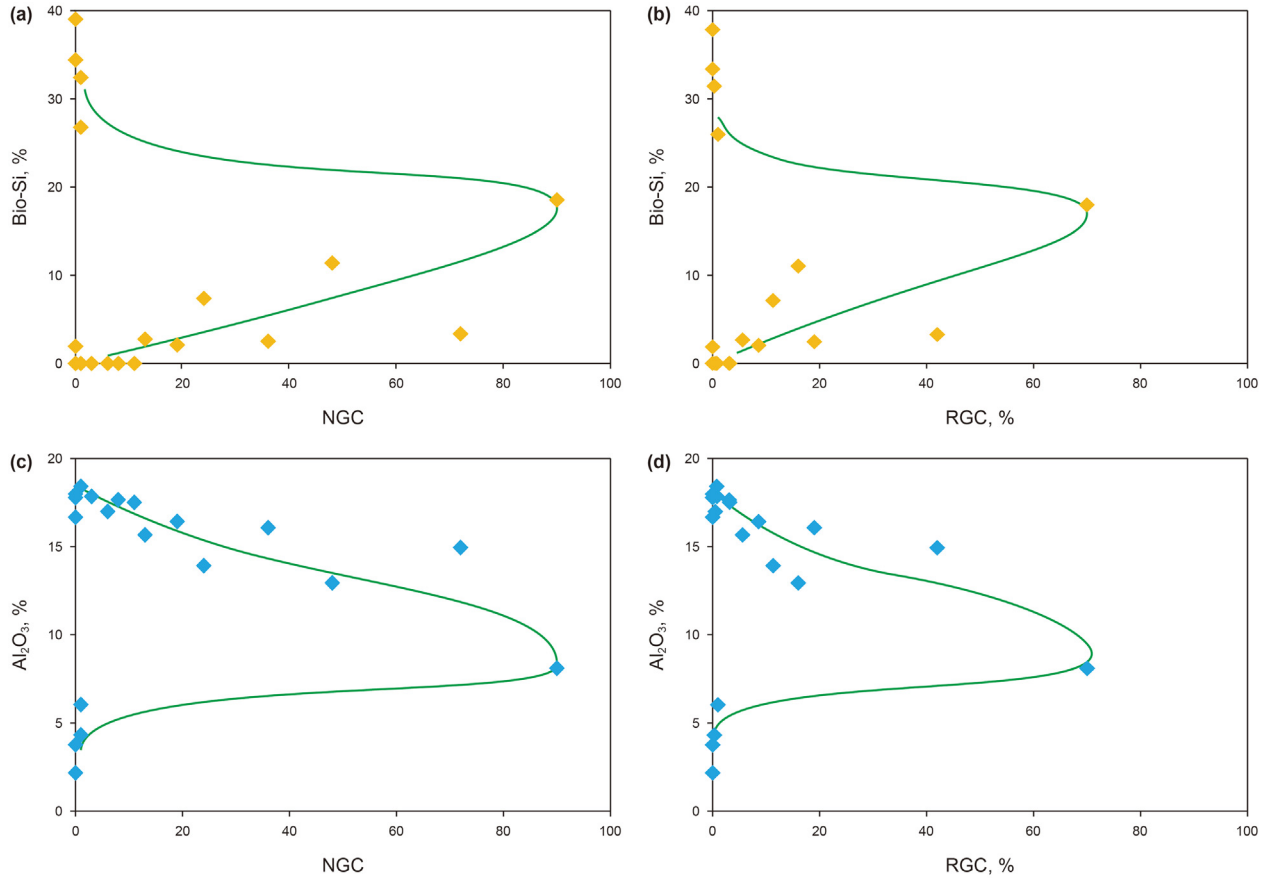

Fig. 12. Bio-Si and Al_2O_3 content versus graptolite abundance for the O_3w-S_1l shale samples in Well Yy3, showing variations in graptolite abundance in shale samples with different biogenic or terrigenous siliceous contents. NGC = number of graptolites on the core bedding surface. RGC = ratio between total graptolite surface area and core bedding surface area.

of organic matter within a greater paleogeographic space. Insufficient terrigenous detrital input accompanied with sea-level rise slows the burial rate of organisms due to the lack of aluminosilicates, and abundant organisms are easily oxidized while slowly settling through the water column (Ibach, 1980; Rimmer, 2004; Lu et al., 2019; Wang et al., 2019). Meanwhile, large planktonic graptolites cannot be transported to a deep-water area over long distances, except for some small fragments. These concepts can illustrate why the TOC value decreases in siliceous shale with higher Bio-Si content and fewer terrigenous siliciclastic deposits formed in an enhanced reductive environment (Figs. 10 and 11), and why mixed siliceous shale with Bio-Si content ranging from 10% to 20% commonly contains abundant organic matter and graptolite fossils (Figs. 11 and 12a, b). However, the TOC of siliceous shale formed in a deep-water environment is commonly greater than that of mixed argillaceous shale because of good organic matter preservation after burial, despite the slightly decreased TOC in siliceous shale caused by a continuous sea-level rise (Figs. 11, 14 and 15).

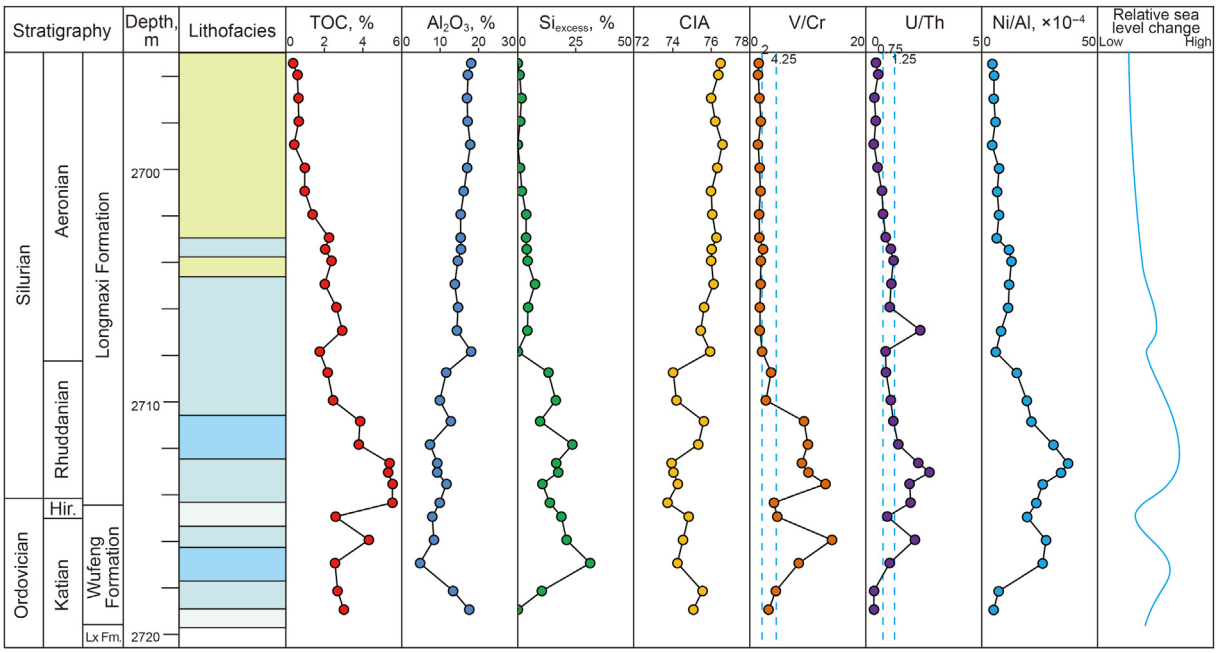

Fig. 13. Vertical variations in different geochemical proxies from O_3w-S_1l shale samples in formations in Well Yy2 (Lx Fm = Lingxiang Formation, and Hir = Hirnantian). V/Cr ratios of 2 and 4.25 and U/Th ratios of 0.75 and 1.25 are used to identify redox conditions and are marked by blue vertical dash lines.

On the contrary, the increased restriction of sedimentary water caused by sea-level drop will restrict nutrient materials migrated from the ocean to the shelf, leading to a decrease in paleoproductivity (Wang et al. 2015, 2019; Dong et al., 2018; Lu et al., 2019). In the semi-enclosed paleoenvironment, although decreasing paleoproductivity may reduce the organisms supply, organic matter will not disperse widely and can be easily concentrated. Furthermore, a slight increase in terrigenous siliciclastic input will benefit organic matter preservation by decreasing the exposure time for oxidation (Rimmer, 2004; Lu et al., 2019). However, once sea-level fall exceeds a certain elevation, terrigenous detrital influx will dilute the organic matter content markedly (Lu et al., 2019), and stronger hydrodynamic conditions and exhaustive bottom water oxidation are not favorable for organism deposition and preservation (Fig. 13). Therefore, some organisms are buried but are still oxidized, and siliceous radiolarians are also not common in mixed shale or mixed argillaceous shale (Fig. 5h and i). For example, the Longmaxi Formation Aeronian shale formed in shallow water generally has a low graptolite abundance and low TOC (Figs. 10 and 12c, d).

For organic matter enrichment in a continental shelf with little influence from hydrothermal activity, we emphasize the controls of organic matter supply and preservation caused by sea-level change and terrigenous input on organic matter accumulation (Ibach, 1980; Gambacorta et al., 2016; Lu et al., 2019). The environment with appropriate sea level and terrigenous input should be most favorable for organic matter enrichment (Fig. 14). In this contribution, the sedimentary environment in the study area corresponding to shale sediments with approximately 8%–10% Al_2O_3 content and 10%–20% Bio-Si content are favorable for organic matter sedimentation and preservation during the Ordovician-Silurian transition (Figs. 10–12). However, the threshold values of Al_2O_3 and Bio-Si content best for organic matter enrichment may change in environments with different paleogeomorphology and provenance systems.

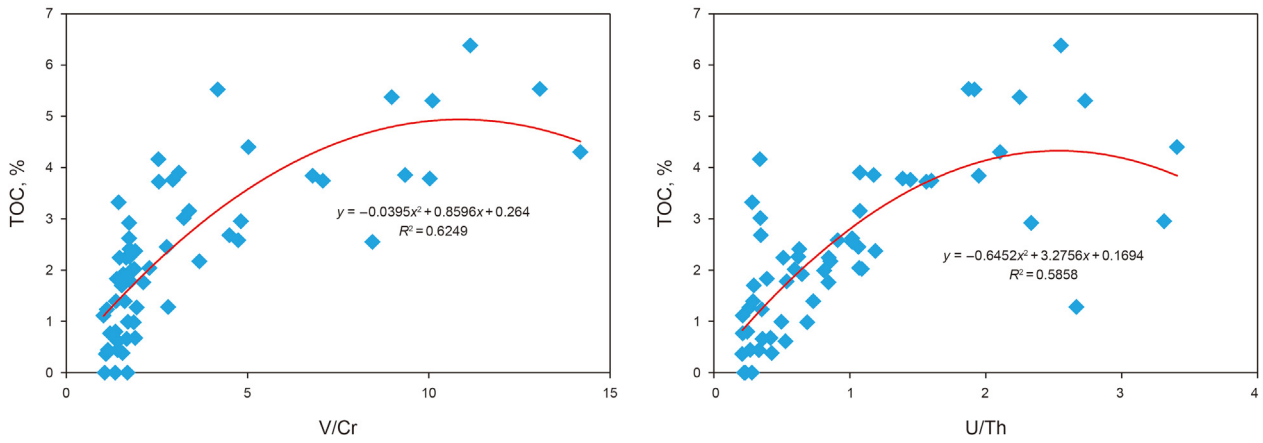

Fig. 14. Cross-plots of TOC versus V/Cr and U/Th for the O_3w-S_1l shale samples showing TOC variations in different redox conditions. Generally, V/Cr ratios <2 or U/Th ratios <0.75 indicate an oxic environment, the U/Th ranges from 0.75 to 1.25 or V/Cr ranges from 2.0 to 4.25 indicates dysoxic environment, and U/Th ratios >1.25 or V/Cr ratios >4.25 indicate anoxic environment.

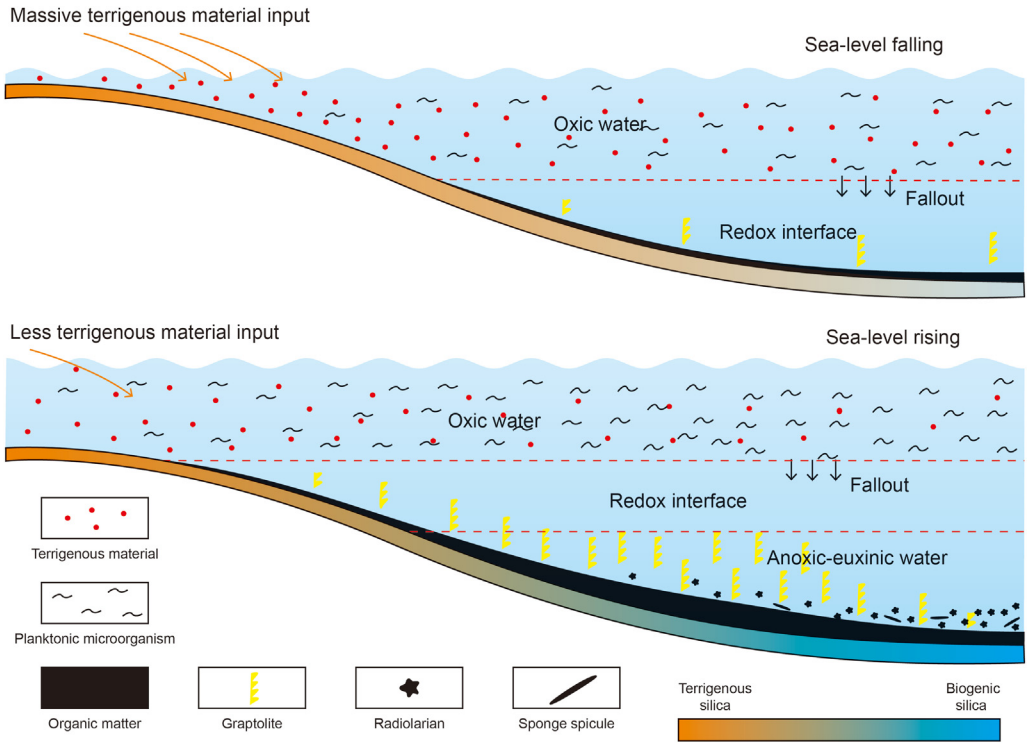

Fig. 15. Sedimentary models for different siliceous materials and organic matter in a semi-enclosed shelf basin with little hydrothermal influence.

6. Conclusions

Bio-Si and terrigenous siliciclastic input are the primary silica sources for the O_3w-S_1l black shale in western Hubei Province, and they exhibit nonlinear correlations with TOC and graptolite abundance, rather than simple linear correlations. Black shale with approximately 8%–10% Al_2O_3 or 10%–20% Bio-Si usually has higher TOC content. Furthermore, TOC exhibits a complex relationship with redox parameters. The nonlinear relationships indicate that organic matter enrichment and distribution of silica with different origins are mainly controlled by sea-level changes and variations in terrigenous input, and using Bio-Si content to evaluate the organic matter enrichment of siliceous shale should be evaluated carefully. Excessive high sea level accompanied with little terrigenous siliciclastic input will decrease the organism supply and slow their burial rate but promote biogenic silica enrichment, while excessive low sea level accompanied with sufficient terrigenous supply will promote organic matter burial but substantially dilute its concentration and lead to an oxidizing environment with abundant terrigenous silica. Therefore, an environment with appropriate sea level and terrigenous input should be most favorable for organic matter accumulation in a continental shelf with little influence of hydrothermal activity, rather than an environment with excessively high sea level, strong reducing conditions, and little terrigenous supply.

Acknowledgements

This study was financially supported by the Key Laboratory of Tectonics and Petroleum Resources of Ministry of Education (China University of Geosciences) (Grant no. TPR-2021-13), the Science and technology research project of Hubei Provincial Department of Education (Grant no. Q20211304) and the National Science and Technology Major Project of China (Grant no. 2016ZX05034001-002; 2017ZX05035001-002). We would like to thank Yangui Li and Jingjing Tang for their help collecting samples. In addition, we appreciate editors and reviewers for the critical and helpful comments and suggestions.

References

Adachi, M., Yamamoto, K., Sugisaki, R., 1986. Hydrothermal chert and associated siliceous rocks from the northern Pacific their geological significance as indication of ocean ridge activity. Sediment. Geol. 47 (1–2), 125–148. https://doi.org/10.1016/0037-0738(86)90075-8.

Algeo, T.J., Maynard, J.B., 2004. Trace-element behavior and redox facies in core shales of Upper Pennsylvanian Kansas-type cyclothems. Chem. Geol. 206 (3–4), 289–318. https://doi.org/10.1016/j.chemgeo.2003.12.009.

Boström, K., 1973. Provenance and accumulation rates of opaline silica, Al, Fe, Ti, Mn, Cu, Ni and Co in Pacific pelagic sediments. Chem. Geol. 11, 123–148. https://doi.org/10.1016/0009-2541(73)90049-1.

Cai, Q.S., Chen, X.H., Zhang, B.M., et al., 2020. Origin of siliceous minerals in the black shale of the Wufeng and Longmaxi Formations in the Yichang area, western Hubei Province: geological significance for shale gas. Acta Geol. Sin. 94 (3), 931–946. https://doi.org/10.3969/j.issn.0001-5717.2020.03.018.

Chen, X., Rong, J.Y., Li, Y., et al., 2004. Facies patterns and geography of the yangtze region, south China, through the ordovician and silurian transition. Palaeogeogr. Palaeoclimatol. Palaeoecol. 204 (3–4), 353–372. https://doi.org/10.1016/S0031-0182(03)00736-3.

Chen, D.Z., Qing, H.R., Yan, X., et al., 2006. Hydrothermal venting and basin evolution (Devonian, South China): constraints from rare earth element geochemistry of chert. Sediment. Geol.. 2006 183 (3–4), 203–216. https://doi.org/10.1016/j.sedgeo.2005.09.020.

Chen, X.H., Zhang, B.M., Chen, L., et al., 2018. Main geological controlling factors and enrichment pattern of shale gas reservoirs in the late ordovician–early silurian strata of yichang, western Hubei Province. Acta Geosci. Sin. 39 (3), 257–268. https://doi.org/10.3975/cagsb.2018.050901 (In Chinese).

Dean, W.E., Leinen, M., Stow, D.A.V., 1985. Classification of deep-sea, fine-grained sediments. J. Sediment. Petrol. 55 (2), 250–256. https://doi.org/10.1111/j.1525-1314.1985.tb00322.x.

Dong, T., Harris, N.B., Ayranci, K., 2018. Relative sea-level cycles and organic matter accumulation in shales of the middle and upper devonian horn river group, northeastern british columbia, Canada: insights into sediment flux, redox conditions, and bioproductivity. Geol. Soc. Am. Bull. 130 (5–6), 859–880. https://doi.org/10.1130/B31851.1.

Dong, T., He, S., Chen, M.F., et al., 2019. Quartz types and origins in the paleozoic Wufeng-Longmaxi Formations, Eastern Sichuan Basin, China: implications for porosity preservation in shale reservoirs. Mar. Petrol. Geol. 106, 62–73. https://doi.org/10.1016/j.marpetgeo.2019.05.002.

Fan, J.X., Melchin, M.J., Chen, X., et al., 2011. Biostratigraphy and geography of the ordovician-silurian lungmachi black shales in South China. Sci. China Earth Sci. 54 (12), 1854–1863. https://doi.org/10.1007/s11430-011-4301-3.
Gambacorta, G., Trincianti, E., Torricelli, S., 2016. Anoxia controlled by relative sea-level changes: an example from the Mississippian Barnett Shale Formation. Palaeogeogr. Palaeoclimatol. Palaeoecol. 459, 306–320. https://doi.org/10.1016/j.palaeo.2016.07.015.
Gorjan, P., Kaiho, K., Fike, D.A., et al., 2012. Carbon- and sulfur-isotope geochemistry of the hirnantian (late ordovician) wangjiawan (riverside) section, south China: global correlation and environmental event interpretation. Palaeogeogr. Palaeoclimatol. Palaeoecol. 337–338, 14–22. https://doi.org/10.1016/j.palaeo.2012.03.021.
Han, C., Jiang, Z.X., Han, M., et al., 2016. The lithofacies and reservoir characteristics of the upper ordovician and lower silurian black shale in the southern sichuan basin and its periphery, China. Mar. Petrol. Geol. 75, 181–191. https://doi.org/10.1016/j.marpetgeo.2016.04.014.
Han, C., Han, M., Jiang, Z.X., et al., 2018. Source analysis of quartz from the upper ordovician and lower silurian black shale and its effects on shale gas reservoir in the southern sichuan basin and its periphery, China. Geol. J. 51, 439–449. https://doi.org/10.1002/gj.3192.
Harris, N.B., Miskimins, J.L., Mnich, C.A., 2011. Mechanical anisotropy in the Woodford shale, Permian Basin: origin, magnitude, and scale. Lead. Edge 30 (3), 284–291. https://doi.org/10.1190/1.3567259.
Huang, H.Y., He, D.F., et al., 2018. Silurian tectonic-sedimentary setting and basin evolution in the Sichuan area, southwest China: implications for palaeogeographic reconstructions. Mar. Petrol. Geol. 92, 403–423. https://doi.org/10.1016/j.marpetgeo.2017.11.006.
Ibach, L.E.J., 1980. Relationship between sedimentation rate and total organic carbon content in ancient marine sediments. AAPG (Am. Assoc. Pet. Geol.) Bull. 66 (2), 170–188. https://doi.org/10.1306/03B59A5D-16D1-11D7-8645000102C1865D.
Ji, W.M., Hao, F., Song, Y., et al., 2020. Organic geochemical and mineralogical characterization of the lower Silurian Longmaxi shale in the southeastern Chongqing area of China: implications for organic matter accumulation. Int. J. Coal Geol. 220. https://doi.org/10.1016/j.coal.2020.103412.
Jiang, T., Jin, Z.J., Liu, G.X., et al., 2019. Source analysis of siliceous minerals and uranium in Early Cambrian shales, South China: significance for shale gas exploration. Mar. Petrol. Geol. 102, 101–108. https://doi.org/10.1016/j.marpetgeo.2018.11.002.
Jones, B., Manning, D.A.C., 1994. A comparison and correlation of different geochemical indices used for the interpretation of depositional environments in ancient mudstones. Chem. Geol. 111 (1–4), 111–129. https://doi.org/10.1016/0009-2541(94)90085-X.
Keil, R.G., Mayer, L.M., 2014. Mineral matrices and organic matter. In: Treatise on Geochemistry, second ed. Elsevier, pp. 337–359. https://doi.org/10.1016/B978-0-08-095975-7.01024-X.
Kennedy, M.J., Pevear, D.R., Hill, R.J., 2002. Mineral surface control of organic carbon in black shale. Science 295, 657–660. https://doi.org/10.1126/science.1066611.
Khan, M.Z., Feng, Q.L., Zhang, K., et al., 2019. Biogenic silica and organic carbon fluxes provide evidence of enhanced marine productivity in the upper Ordovician-Lower Silurian of South China. Palaeogeogr. Palaeoclimatol. Palaeoecol. 534, 109278. https://doi.org/10.1016/j.palaeo.2019.109278.
Lewan, M.D., Maynard, J.B., 1982. Factors controlling enrichment of vanadium and nickel in the bitumen of organic sedimentary rocks. Geochem. Cosmochim. Acta 46 (12), 2547–2560. https://doi.org/10.1016/0016-7037(82)90377-5.
Li, G.S., Wang, F., Liang, Q., Li, J.L., 2003. Estimation of ocean primary productivity by remote sensing and introduction to spatio-temporal variation mechanism for the east China sea. Acta Geograph. Sin. 58, 483–493. https://doi.org/10.1007/s11769-003-0089-1 (In Chinese).
Li, T.Y., He, S., He, Z.L., et al., 2012. Reconstruction of tectonic uplift and thermal history since mesozoic in the dangyang synclinorium of the central yangtze area. Acta Pet. Sin. 33 (2), 213–224. https://doi.org/10.7623/syxb201202005 (In Chinese).
Li, Y.J., Liu, H., Zhang, L.H., et al., 2013. Lower limits of evaluation parameters for the lower Paleozoic Longmaxi shale gas in southern Sichuan Province. Sci. China Earth Sci. 56, 710–717. http://377.rm.cglhub.com/10.1007/s11430-013-4579-4.
Li, Y.F., Fan, T.L., Zhang, J.C., et al., 2015. Geochemical changes in the Early Cambrian interval of the Yangtze Platform, South China: implications for hydrothermal influences and paleocean redox conditions. J. Asian Earth Sci. 109, 100–123. https://doi.org/10.1016/j.jseaes.2015.05.003.
Li, Y.F., Zhang, T.W., Ellis, G.S., et al., 2017. Depositional environment and organic matter accumulation of upper ordovician-lower silurian marine shale in the upper yangtze platform, south China. Palaeogeogr. Palaeoclimatol. Palaeoecol. 466, 252–264. https://doi.org/10.1016/j.palaeo.2016.11.037.
Li, Y.F., Sun, W., Liu, X.W., et al., 2018. Study of the relationship between fractures and highly productive shale gas zones, Longmaxi Formation, Jiaoshiba area in eastern Sichuan. Petrol. Sci. 15, 498–509. http://377.rm.cglhub.com/10.1007/s12182-018-0249-7.
Li, D.L., Li, R.X., Tan, C.Q., et al., 2019. Origin of silica, paleoenvironment, and organic matter enrichment in the Lower Paleozoic Niutitang and Longmaxi formations of the northwestern Upper Yangtze Plate: significance for hydrocarbon exploration. Mar. Petrol. Geol. 103, 404–421. https://doi.org/10.1016/j.marpetgeo.2019.02.025.
Liu, Y., Li, C., Algeo, T.J., et al., 2016. Global and regional controls on marine redox changes across the Ordovician-Silurian boundary in South China. Palaeogeogr. Palaeoclimatol. Palaeoecol. 463, 180–191. https://doi.org/10.1016/j.palaeo.2016.10.006.
Liu, Z.H., Algeo, T.J., Guo, X.S., et al., 2017. Paleo-environmental cyclicity in the early silurian yangtze sea (South China): tectonic or glacio-eustatic control? Palaeogeogr. Palaeoclimatol. Palaeoecol. 466, 59–76. https://doi.org/10.1016/j.palaeo.2016.11.007.
Liu, B., Schieber, J., Mastalerz, M., et al., 2019. Organic matter content and type variation in the sequence stratigraphic context of the Upper Devonian New Albany Shale, Illinois Basin. Sediment. Geol. 383, 101–120. https://doi.org/10.1016/j.sedgeo.2019.02.004.
Liu, G.H., Zhai, G.Y., Zou, C.N., et al., 2019. A comparative discussion of the evidence for biogenic silica in Wufeng-Longmaxi siliceous shale reservoir in the Sichuan basin, China. Mar. Petrol. Geol. 109, 70–87. https://doi.org/10.1016/j.marpetgeo.2019.06.016.
Lu, Y.B., Jiang, S., Lu, Y.C., et al., 2019. Productivity or preservation? The factors controlling the organic matter accumulation in the late Katian through Hirnantian Wufeng organic-rich shale, South China. Mar. Petrol. Geol. 109, 22–35. https://doi.org/10.1016/j.marpetgeo.2019.06.007.
Luo, Q.Y., Zhong, N.N., Dai, N., et al., 2016. Graptolite-derived organic matter in the Wufeng-Longmaxi formations (Upper Ordovician-Lower Silurian) of southeastern Chongqing, China: implications for gas shale evaluation. Int. J. Coal Geol. 153, 87–98. https://doi.org/10.1016/j.coal.2015.11.014.
Ma, X.H., Xie, J., Yong, R., et al., 2020. Geological characteristics and high production control factors of shale gas reservoirs in Silurian Longmaxi Formation, southern Sichuan Basin, SW China. Petrol. Explor. Dev. 47 (5), 901–915. https://doi.org/10.1016/S1876-3804(20)60105-7.
McLennan, S.M., 1993. Weathering and global denudation. J. Geol.,1993 101, 295–303. https://doi.org/10.1086/648222.
Milliken, K.L., Olson, T., 2017. Silica diagenesis, porosity evolution, and mechanical behavior in siliceous mudstones, Moway Shale (Cretaceous), Rocky Mountains, U.S.A. J. Sediment. Res. 87, 366–387. https://doi.org/10.2110/jsr.2017.24.
Milliken, K.L., Ergene, S.M., Ozka, A., 2016. Quartz types, authigenic and detrital, in the upper cretaceous eagle ford formation, south Texas, USA. Sediment. Geol. 339, 273–288. https://doi.org/10.1016/j.sedgeo.2016.03.012.
Murphy, A.E., Sageman, B.B., Hollander, et al., 2000. Black shale deposition and faunal overturn in the Devonian Appalachian Basin: Clastic starvation, seasonal water-column mixing, and efficient biolimiting nutrient recycling. Paleoceanogr. Paleoclimatol. 15 (3), 280–291. https://doi.org/10.1029/1999PA000445.
Murray, R.W., 1994. Chemical criteria to identify the depositional environment of chert: General principles and applications. Sediment. Geol. 90, 213–232. https://doi.org/10.1016/0037-0738(94)90039-6.
Murray, R.W., Leinen, M., 1996. Scavenged excess aluminum and its relationship to bulk titanium in biogenic sediment from the central equatorial Pacific Ocean. Geochem. Cosmochim. Acta 60 (20), 3869–3878. https://doi.org/10.1016/0016-7037(96)00236-0.
Murry, R.W., Buchholtz, T., Brink, M.R., et al., 1991. Rare earth, major, and trace elements in chert from the Franciscan Complex and Monterey Group, California: Assessing REE sources to fine-grained marine sediments. Geochem. Cosmochim. Acta 55 (7), 1875–1895. https://doi.org/10.1016/0016-7037(91)90030-9.
Nelson, D.M., Paul, T., Brzezinski, M.A., et al., 1995. Production and dissolution of biogenic silica in the ocean: Revised global estimates, comparison with regional data and relationship to biogenic sedimentation. Global Biogeochem. Cycles 9 (3), 359–372. https://doi.org/10.1029/95GB01070.
Nesbitt, H.W., Young, G.M., 1982. Early Proterozoic climates and plate motions inferred from major element chemistry of lutites. Nature 299, 715–717. https://doi.org/10.1038/299715a0.
Olivarez, A.M., Owen, R.M., 1989. REE/Fe variations in hydrothermal sediments: Implications for the REE content of seawater. Geochem. Cosmochim. Acta 53 (3), 757–762. https://doi.org/10.1016/0016-7037(89)90019-7.
Pan, X.P., Zhang, G.Z., Chen, J.J., 2020. The construction of shale rock physics model and brittleness prediction for high-porosity shale gas-bearing reservoir. Petrol. Sci. 17, 658–670. http://377.rm.cglhub.com/10.1007/s12182-020-00432-2.
Platt, T., Sathyendranath, S., 1988. Oceanic primary production: Estimation by remote sensing at local and regional scales. Science 241, 1613–1620. https://doi.org/10.1126/science.241.4873.1613.
Porter, S.J., Selby, D., Cameron, V., 2014. Characterising the nickel isotopic composition of organic-rich marine sediments. Chem. Geol. 387, 12–21. https://doi.org/10.1016/j.chemgeo.2014.07.017.
Price, J.R., Velbel, M.A., 2003. Chemical weathering indices applied to weathering profiles developed on heterogeneous felsic metamorphic parent rocks. Chem. Geol. 202, 397–416. https://doi.org/10.1016/j.chemgeo.2002.11.001.
Qiu, Z., Wang, Q.C., 2011. Geochemical evidence for submarine hydrothermal origin of the Middle-Upper Permian chert in Laibin of Guangxi, China. Sci. China Earth Sci. 54 (7), 1011–1023. https://doi.org/10.1007/s11430-011-4198-x.
Qiu, Z., Tan, X., Lu, B., et al., 2018. Geochemical Characteristics of Cherts from the Wufeng and Longmaxi Formations in the Wuxi Area, Sichuan Basin. Bull. China Soc. Mineral Petrol. Geochem. 37 (5), 880–887. https://doi.org/10.19658/j.issn.1007-2802.2018.37.008 (In Chinese).
Rimmer, S.M., 2004. Geochemical paleoredox indicators in Devonian-Mississippian black shales, Central Appalachian Basin (USA). Chem. Geol. 206 (3–4), 373–391. https://doi.org/10.1016/j.chemgeo.2003.12.029.
Rong, J.Y., Chen, X., Harper, D.A.T., 2002. The latest Ordovician Hirnantia Fauna (Brachiopoda) in time and space. Lethaia 35 (3), 231–249. https://doi.org/10.1111/j.1502-3931.2002.tb00081.x.
Ross, D.J.K., Bustin, R.M., 2009. Investigating the use of sedimentary geochemical

proxies for paleoenvironment interpretation of thermally mature organic-rich strata: Examples from the Devonian-Mississippian shales, Western Canadian Sedimentary Basin. Chem. Geol. 260 (1–2), 1–19. https://doi.org/10.1016/j.chemgeo.2008.10.027.

Sageman, B.B., Murphy, A.E., Werne, J.P., et al., 2003. A tale of shales: the relative roles of production, decomposition, and dilution in the accumulation of organic-rich strata, Middle–Upper Devonian, Appalachian basin. Chem. Geol. 195 (1–4), 229–273.

Schieber, J., 2016. Experimental testing of the transport-durability of shale lithics and its implications for interpreting the rock record. Sediment. Geol. 331, 162–169. https://doi.org/10.1016/j.sedgeo.2015.11.006.

Schieber, J., Krinsley, D., Riciputi, L., 2000. Diagenetic origin of quartz silt in mudstones and implications for silica cycling. Nature 406, 981–985. https://doi.org/10.1038/35023143.

Su, W.B., Li, Z.M., Ettensohn, F.R., et al., 2007. Tectonic and eustatic control on the distribution of black-shale source beds in the Wufeng and Longmaxi formations (Ordovician-Silurian), South China. Front. Earth Sci. China 1, 470–481. http://377.rm.cglhub.com/10.1007/s11707-007-0058-6.

Su, W.B., Huff, W.D., Ettensohn, F.R., et al., 2009. K-bentonite, black-shale and flysch successions at the Ordovician-Silurian transition, South China: Possible sedimentary responses to the accretion of Cathaysia to the Yangtze Block and its implications for the evolution of Gondwana. Gondwana Res. 15 (1), 111–130. https://doi.org/10.1016/j.gr.2008.06.004.

Taylor, S.R., Mcclennans, M., 1985. The Continental Crust: Its Composition and Evolution. In: An Examination of the Geochemical Record Preserved in Sedimentary Rocks. Blackwell Scientific publication, Oxford, p. 31.

Tribovillard, N., Algeo, T.J., Lyons, T., et al., 2006. Trace metals as paleoredox and paleoproductivity proxies: An update. Chem. Geol. 232 (1–2), 12–32. https://doi.org/10.1016/j.chemgeo.2006.02.012.

Wang, Y.M., Dong, D.Z., Yang, H., et al., 2014. Quantitative characterization of reservoir space in the Lower Silurian Longmaxi Shale, southern Sichuan, China. Sci. China Earth Sci. 57, 313–322. http://377.rm.cglhub.com/10.1007/s11430-013-4645-y.

Wang, Y.M., Dong, D.Z., Li, X.J., et al., 2015. Stratigraphic sequence and sedimentary characteristics of Lower Silurian Longmaxi Formation in Sichuan Basin and its peripheral areas. Nat. Gas. Ind. B 2 (2–3), 222–232. https://doi.org/10.1016/j.ngib.2015.07.014.

Wang, Y.X., Xu, S., Hao, F., et al., 2019. Geochemical and petrographic characteristics of Wufeng-Longmaxi shales, Jiaoshiba area, southwest China: Implications for organic matter differential accumulation. Mar. Petrol. Geol. 102, 138–154. https://doi.org/10.1016/j.marpetgeo.2018.12.038.

Wignall, P.B., Myers, K.J., 1988. Interpreting benthic oxygen levels in mudrocks: A new approach. Geology 16 (5), 452–455. https://doi.org/10.1130/0091-7613(1988)016<0452:IBOLIM>2.3.CO;2.

Wright, J., 2001. Making loess-sized quartz silt: Data from laboratory simulations and implications for sediment transport pathways and the formation of 'desert' loess deposits associated with the Sahara. Quat. Int. 76–77, 7–19. https://doi.org/10.1016/S1040-6182(00)00085-9.

Wu, Y.W., Tian, H., Gong, D.J., et al., 2020. Paleo-environmental variation and its control on organic matter enrichment of black shales from shallow shelf to slope regions on the Upper Yangtze Platform during Cambrian Stage 3. Palaeogeogr. Palaeoclimatol. Palaeoecol. 545. https://doi.org/10.1016/j.palaeo.2020.109653.

Xi, Z.D., Tang, S.H., Zhang, S.H., et al., 2019. Characterization of quartz in the Wufeng Formation in northwest Hunan Province, south China and its implications for reservoir quality. J. Petrol. Sci. Eng. 179, 979–996. https://doi.org/10.1016/j.petrol.2019.04.051.

Xiao, X.M., Wei, Q., Gai, H.F., et al., 2015. Main controlling factors and enrichment area evaluation of shale gas of the Lower Paleozoic marine strata in south China. Petrol. Sci. 12, 573–586. https://doi.org/10.1007/s12182-015-0057-2.

Yamamoto, K., 1987. Geochemical characteristics and depositional environments of cherts and associated rocks in the Franciscan and Shimanto Terranes. Sediment. Geol. 52 (1–2), 65–108. https://doi.org/10.1016/0037-0738(87)90017-0.

Yan, D.T., Chen, D.Z., Wang, Q.C., et al., 2010. Large-scale climatic fluctuations in the latest Ordovician on the Yangtze block, south China. Geology 38 (7), 599–602. https://doi.org/10.1130/G30961.1.

Yan, D.T., Chen, D.Z., Wang, Z.Z., et al., 2019. Climatic and oceanic controlled deposition of Late Ordovician-Early Silurian black shales on the North Yangtze platform, South China. Mar. Petrol. Geol. 110, 112–121. https://doi.org/10.1016/j.marpetgeo.2019.06.040.

Yang, X.R., Yan, D.T., Wei, X.S., et al., 2018. Different formation mechanism of quartz in siliceous and argillaceous shales: A case study of Longmaxi Formation in South China. Mar. Petrol. Geol. 94, 80–94. https://doi.org/10.1016/j.marpetgeo.2018.03.036.

Yang, L., Ran, B., Han, Y.Y., et al., 2019. Sedimentary environment controls on the accumulation of organic matter in the Upper Ordovician Wufeng–Lower Silurian Longmaxi mudstones in the Southeastern Sichuan Basin of China. Petrol. Sci. 16, 44–57. http://377.rm.cglhub.com/10.1007/s12182-018-0283-5.

Yang, R., Hu, Q.H., Yi, J.Z., et al., 2019. The effects of mineral composition, TOC content and pore structure on spontaneous imbibition in Lower Jurassic Dongyuemiao shale reservoirs. Mar. Petrol. Geol. 109, 268–278. https://doi.org/10.1016/j.marpetgeo.2019.06.003.

Yang, X.R., Yan, D.T., Zhang, L.W., et al., 2020. The depositional mechanism of organic-rich siliceous shales in Upper Yangtze area: Response to the Kwangsian Orogeny in South China. J. Petrol. Sci. Eng. 192, 107310. https://doi.org/10.1016/j.petrol.2020.107310.

Zeng, W.T., Zhang, J.C., Ding, W.L., et al., 2013. Fracture development in Paleozoic shale of Chongqing area (South China). Part one: Fracture characteristics and comparative analysis of main controlling factors. J. Asian Earth Sci. 75, 251–266. https://doi.org/10.1016/j.jseaes.2013.07.015.

Zhan, R.B., Liu, J.B., Percival, I.G., et al., 2010. Biodiversification of Late Ordovician Hirnantia fauna on the Upper Yangtze platform, South China. Sci. China D: Earth Sci. 53, 1800–1810. https://doi.org/10.1007/s11430-010-4071-3.

Zhang, K., Li, Z., Jiang, S., et al., 2018. Comparative analysis of the siliceous source and organic matter enrichment mechanism of the upper Ordovician-Lower Silurian shale in the Upper-Lower Yangtze area. Minerals 8 (7), 283. https://doi.org/10.3390/min8070283.

Zhang, Y.Y., He, Z.L., Jiang, S., et al., 2018. Controls on the organic carbon content of the lower Cambrian black shale in the southeastern margin of Upper Yangtze. Petrol. Sci. 15 (4), 709–721. https://doi.org/10.1007/s12182-018-0262-x.

Zhang, J.F., Xu, H., Zhou, Z., et al., 2019. Geological characteristics of shale gas reservoir in Yichang area, western Hubei. Acta Pet. Sin. 40 (8), 887–899. https://doi.org/10.7623/syxb201908001 (In Chinese).

Zhang, L.C., Xiao, D.S., Lu, S.F., et al., 2019. Effect of sedimentary environment on the formation of organic-rich marine shale: Insights from major/trace elements and shale composition. Int. J. Coal Geol. 204, 34–50. https://doi.org/10.1016/j.coal.2019.01.014.

Zhao, J.H., Jin, Z.J., et al., 2016. The genesis of quartz in Wufeng-Longmaxi gas shales, Sichuan Basin. Nat. Gas Geosci. 27 (2), 377–386. https://doi.org/10.11764/j.issn.1672-1926.2016.02.0377 (In Chinese).

Zhao, J.H., Jin, Z.J., Jin, Z.K., et al., 2017a. Mineral types and organic matters of the Ordovician-Silurian Wufeng and Longmaxi Shale in the Sichuan Basin, China: Implications for pore systems, diagenetic pathways, and reservoir quality in fine-grained sedimentary rocks. Mar. Petrol. Geol. 86, 655–674. https://doi.org/10.1016/j.marpetgeo.2017.06.031.

Zhao, J.H., Jin, Z.K., Jin, Z.J., et al., 2017b. Origin of authigenic quartz in organic-rich shales of the Wufeng and Longmaxi formations in the Sichuan basin, south China: Implications for pore evolution. J. Nat. Gas Sci. Eng. 38, 21–38. https://doi.org/10.1016/j.jngse.2016.11.037.

Zhou, Y.Z., Chown, E.H., Guha, J., et al., 2006. Hydrothermal origin of Late Proterozoic bedded chert at Gusui, Guangdong, China: petrological and geochemical evidence. Sedimentology 41, 605–619. https://doi.org/10.1111/j.1365-3091.1994.tb02013.x.